Informes Técnicos Ciemat **1358**
Abril, 2015

Magnet Cycles and Stability Periods of the CMS Structures from 2008 to 2013 as Observed by the Link Alignment System

CIEMAT
Madrid

P. Arce
J.M. Barcala
E. Calvo
A. Ferrando
M.I. Josa
A. Molinero
J. Navarrete
J. C. Oller

IFCA-CSIC-UC
Santander

J. Brochero
A. Calderón
M.G. Fernández
G. Gómez
F.J. González-Sánchez
C. Martínez-Rivero
F. Matorras
T. Rodrigo
R. Sancibrián
L. Scodellaro
M. Sobrón
F. Viadero
I. Vila
A.L. Virto

Univ. Oviedo
Oviedo

J. Fernández

GOBIERNO DE ESPAÑA
MINISTERIO DE ECONOMÍA Y COMPETITIVIDAD
Ciemat
Centro de Investigaciones Energéticas, Medioambientales y Tecnológicas

Informes Técnicos Ciemat **1358**
Abril, 2015

Magnet Cycles and Stability Periods of the CMS Structures from 2008 to 2013 as Observed by the Link Alignment System

CIEMAT
Madrid

P. Arce
J.M. Barcala
E. Calvo
A. Ferrando
M.I. Josa
A. Molinero
J. Navarrete
J.C. Oller

IFCA-CSIC-UC
Santander

J. Brochero
A. Calderón
M.G. Fernández
G. Gómez
F.J. González-Sánchez
C. Martínez-Rivero
F. Matorras
T. Rodrigo
R. Sancibrián
L. Scodellaro
M. Sobrón
F. Viadero
I. Vila
A.L. Virto

Univ. Oviedo
Oviedo

J. Fernández

Departamento de Investigación Básica

Toda correspondencia en relación con este trabajo debe dirigirse al Servicio de Información y Documentación, Centro de Investigaciones Energéticas, Medioambientales y Tecnológicas, Ciudad Universitaria, 28040-MADRID, ESPAÑA.

Las solicitudes de ejemplares deben dirigirse a este mismo Servicio.

Los descriptores se han seleccionado del Thesauro del DOE para describir las materias que contiene este informe con vistas a su recuperación. La catalogación se ha hecho utilizando el documento DOE/TIC-4602 (Rev. 1) Descriptive Cataloguing On-Line, y la clasificación de acuerdo con el documento DOE/TIC.4584-R7 Subject Categories and Scope publicados por el Office of Scientific and Technical Information del Departamento de Energía de los Estados Unidos.

Catálogo general de publicaciones oficiales
http://www.060.es

Depósito Legal: M-26385-2011
ISSN: 1135-9420
NIPO: 721-15-030-4

Editorial CIEMAT

CLASIFICACIÓN DOE Y DESCRIPTORES

S70

PARTICLES; MAGNETIC FIELDS; ALIGMENT; STABIBLITY; MECHANICAL STRUCTURES; MUONS; SOLENOIDS

Magnet Cycles and Stability Periods of the CMS Structures from 2008 to 2013 as Observed by the Link Alignment System

Arce, P.; Barcala, J.M.; Calvo, E.; Ferrando, A.; Josa, M.I.; Molinero, A.;
Navarrete, J. and Oller, J.C.
CIEMAT* (Madrid, Spain)
Brochero, J.; Calderón, A.; Fernández, M.G.; Gómez, G.; González-Sánchez, F.J.;
Martínez-Rivero, C.; Matorras, F.; Rodrigo, T.; Scodellaro, L.; Sobrón, M.; Vila, I. and Virto, A.L.
IFCA-CSIC-UC** (Santander, Spain)
Sancibrián, R. and Viadero, F.
University of Cantabria (Santander, Spain)
Fernández, J.
University of Oviedo (Oviedo, Spain)***

74 pp. 43 figs. 25 tabs. 17 refs.

Abstract:
In this document Magnet Cycles and Stability Periods of the CMS Experiment are studied with the recorded Alignment Link System data along the 2008 to 2013 years of operation. The motions of the mechanical structures due to the magnetic field forces are studied including an in-depth analysis of the relative distance between the endcap structures and the central Tracker body during the Stability Periods to verify the mechanical stability of the detector during the physics data taking.

Ciclos de Campo Magnético y Periodos de Estabilidad de las Estructuras del Experimento CMS de 2008 a 2013 Observados por el Sistema de Alineamiento

Arce, P.; Barcala, J.M.; Calvo, E.; Ferrando, A.; Josa, M.I.; Molinero, A.;
Navarrete, J. and Oller, J.C.
CIEMAT* (Madrid, Spain)
Brochero, J.; Calderón, A.; Fernández, M.G.; Gómez, G.; González-Sánchez, F.J.;
Martínez-Rivero, C.; Matorras, F.; Rodrigo, T.; Scodellaro, L.; Sobrón, M.; Vila, I. and Virto, A.L.
IFCA-CSIC-UC** (Santander, Spain)
Sancibrián, R. and Viadero, F.
University of Cantabria (Santander, Spain)
Fernández, J.
University of Oviedo (Oviedo, Spain)***

74 pp. 43 figs. 25 tabs. 17 refs.

Resumen:
En este documento se estudian los Ciclos de Campo Magnético y los Periodos de Estabilidad a campo constante utilizando los datos del Sistema de Alineamiento Link tomados en los años 2008 a 2013. Los movimientos de las estructuras mecánicas son estudiados, incluyendo un análisis detallado del movimiento relativo entre las estructuras de cierre y el detector central de trazas para verificar que el detector fue mecánicamente estable durante la toma de datos de física.

---

*Under CICYT (Spain) Grant: FPA 2011-29237-C02-01.
**Under CICYT (Spain) Grant: FPA 2011-28694-C02-01.
***Under CICYT (Spain) Grant: FPA 2011-28694-C02-02.

1. Introduction

A major part of the Compact Muon Solenoid detector (CMS) [1-4] is a powerful muon spectrometer [3] for the identification and measurement of muons in a very wide energy range, from a few GeV up to several TeV. Disregarding the low angle calorimeters, CMS has a cylindrical symmetry around the LHC beam pipe, an overall diameter of 15 m, a total length of 21.6 m and weighs 12.5 kt (mainly iron). At its heart, a 13 m long, 6 m inner diameter superconducting solenoid [2] provides a 3.8 T field along the beam axis and a bending power of about 12 Tm in the transverse plane. The return field is captured through 1.5 m of iron layers, allowing four muon stations to be integrated, both in the barrel and in the end-cap regions, to ensure full geometrical coverage.

The accuracy required in the position of the muon chambers is driven by the resolution demanded in the momentum measurement of high energy muons. CMS is designed to achieve a combined (Muon System [3] and Tracker [4]) momentum resolution of 0.5 – 1% for $p_T \approx 10$ GeV, 1.5 – 5% for $p_T \approx 100$ GeV and 5 – 20% for $p_T \approx 1$ TeV for the region $|\eta| < 2.4$. This design accuracy requires the knowledge of the position of the chambers with a precision *comparable* to their resolution.

Several simulation studies were performed [5] in order to quantify the importance of muon chamber alignment in the momentum resolution. For the most important coordinate from the physics point of view, (RΦ), the alignment system should reconstruct the position of the chambers within 150 – 300 μm for MB1 – MB4 and within 75 – 200 μm for ME1 – ME4. The tighter constraints correspond to MB1 and ME1 since the magnetic bending in the yoke is reversed with respect to the inner magnetic field and hence the largest bending is to be measured in the first stations. Since these stations are located at the border of the magnet they allow, in combination with the Tracker hits, to exploit the full bending space in the CMS experiment.

When CMS is in operation, the movements and deflections of the muon spectrometer may exceed 100 μm. To monitor these movements, CMS is instrumented with an opto-mechanical alignment system that performs a continuous and precise measurement of the relative position of the muon chambers amongst themselves as well as the position of the muon spectrometer with respect to the tracker, assumed to be a rigid body. The information provided by the alignment system is used for the off-line track reconstruction.

In a previous document [6] the alignment system was presented and, using the first data taken by the Link Alignment System during the two phases of the 2006 Magnet Test and Cosmic Challenge, the effects of the ramp up and down in magnetic field were studied and it was shown that the Link system obtains geometrical reconstructions of relative spatial locations and angular orientations between the muon chambers and the tracker body with a resolution better than 150 μm for distances and about 40 μrad for angles.

The structural equilibrium was also investigated [7]. Using alignment system data from the years 2008 and 2009, it was found that once the magnetic field intensity reaches 3.8 T, provided that the current in the coils remains unaltered, the mechanical structures reach equilibrium within the first 24 h. By structural equilibrium it is understood that any displacement in any direction (axial or radial) will remain within the distance sensors resolution: ± 40 μm and any rotation within the tiltmeters

resolution: ± 40 μrad. These structural equilibrium periods will be called *Stability Periods*.

However, and as also explained in Ref. [7], a long term monitoring of 2010 link data showed an apparent exception to the expected structural equilibrium: during the periods at constant B = 3.8T and after the first 24 hours, the central part of the YE±1 endcap structures seem to have an *accordion-like* motion of amplitude in the range 200 – 250 μm, towards and away from the CMS geometrical centre.

This document presents a summary of the CMS Link Alignment monitoring of the relative motions of those two structures during the full period from 2008 to 2013, including the large movements during complete magnet cycles and the small ones during the Stability Periods.

Magnet Cycles and *Stability Periods* during this six-year survey are enumerated and investigated. A *Magnet Cycle* is defined as the time elapsed between the switching of the current in the coils on and off. The switch off is occasionally uncontrolled (fast dump): the current in the coils may pass from ~18000 A to 0 A in a few seconds. When this happens the magnet takes a minimum of a couple of days to restart working properly. The *Stability Periods,* at constant working magnetic fields, occurred at 4T in the first year of operation and at 3.8 T in the subsequent years. Cosmic rays, proton-proton or heavy ion collision data are taken during the *Stability Periods*.

The present study includes the incidence of eventual temperature changes in the calculation of the relative distances between the endcap disks of the forward muon chambers and the central tracker with the aim of finding a possible explanation to the recorded motions surpassing the ± 40 μm resolutions.

This document is organized as follows: a short description of the CMS Alignment System is given in section 2. Magnet Cycles and Stability Periods are presented in Section 3. The results of the monitoring of the distances between the Link Disks and its corresponding Alignment Rings, Z(LD-AR), during the various Magnets Cycles along the 2008-2013 operations, are presented in Section 4. Section 5 is devoted to an in-depth study of the relative ΔZ(LD-AR) distances during the Stability Periods in these six years of operation, with special analysis of the monitored temperature in the volume between the Link Disks and the Alignment Rings and the discussion of the possible correlations between both quantities. For completeness some examples of recorded data from the monitoring of the variables assumed to be mechanically stable are shown in Section 6. Finally, summary and conclusions are given in Section 7.

2. The CMS Alignment System

A longitudinal view of one quadrant of the CMS experiment showing the various detectors is given in Fig. 1. Different muon detection technologies are employed for the central and the endcap regions, due to the different conditions of the magnetic field in terms of intensity and homogeneity. In the barrel region, surrounding the coil of the solenoid, four concentric stations of drift tube (DT) chambers (named MB1 to MB4), are inserted in the five wheels that constitute the return iron yoke. A muon chamber is built of three superlayers. Each superlayer in turn is made of four layers of drift cells, being the drift cell the basic detection unit. Drift times are translated into local space positions with a single hit resolution of 250 μm. Superlayers are arranged such that they measure the muon in two orthogonal coordinates: two superlayers measure the muon in the bending plane and the third superlayer measures it along the beam axis direction.

The mechanical design of a drift chamber is driven by the 100 μm spatial precision requirement in the determination of the track position in the bending plane. Track segments are obtained by linear fits to the reconstructed hits in each coordinate. The DT chambers are subject to variable residual magnetic fields below 0.4 T for all the stations except for the innermost MB1 chambers closest to the endcaps, where the field reaches 0.8 T.

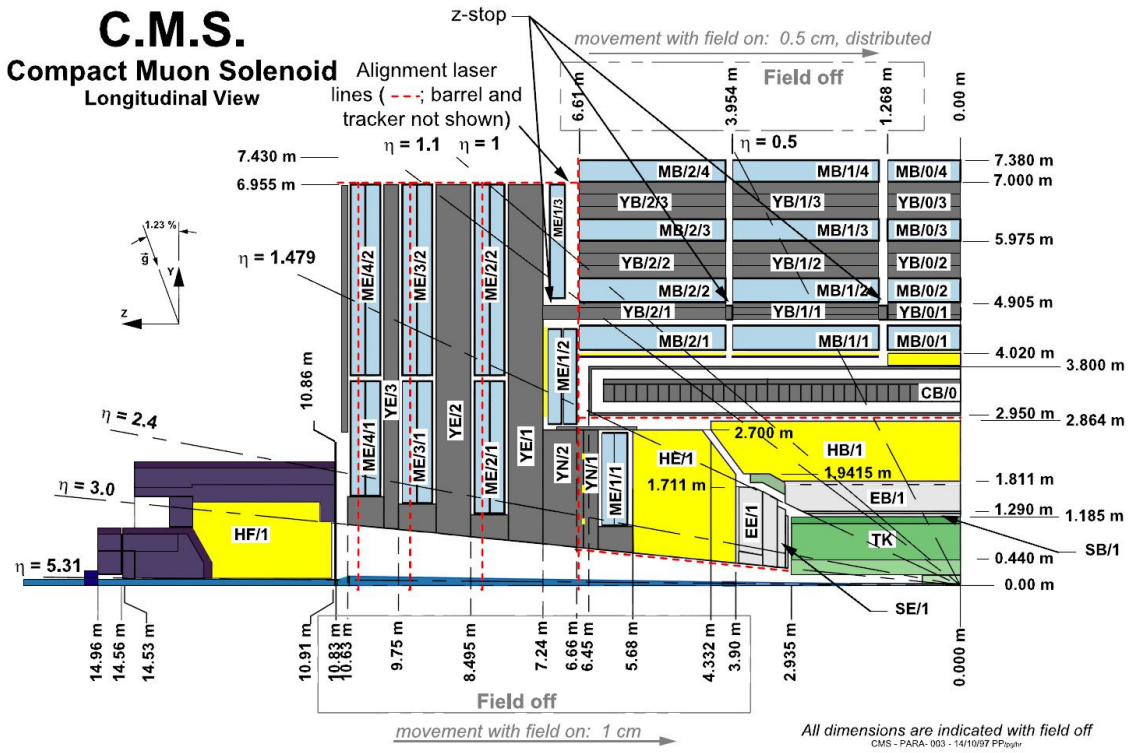

Fig. 1: *Longitudinal view of one quadrant of the CMS detector. The position of the Z-stops is indicated. Laser lines (dashed lines) used for the Alignment System are also shown, except for the barrel region.*

At both CMS endcap sides there are four layers of muon chambers, named ME1 to ME4. In the endcap regions the magnetic field is typically high and very inhomogeneous due to its bending to feed the barrel yoke. In addition, at the level of the ME1 chambers the field intensity may be as high as 3 T. To cope with this and with the high particle fluxes in these regions, different gas ionization detectors called Cathode Strip Chambers (CSCs) are used for this region. The CSCs are multi-wire proportional chambers in which one cathode plane is segmented into strips running across wires, giving 2D information of the particle passage. Due to the intense magnetic field, the muon trajectories bend more in the vicinity of the first endcap station, where a higher precision is required (75 μm). For the rest of the chambers the necessary precision is about 150 μm.

Layers of Resistive Plate Chambers (RPCs), both in the barrel and in the endcaps, complement the muon spectrometer. They are used mainly for trigger purposes as their time resolution is better than 2 ns, although their hits may also participate in the muon

track reconstruction. The RPCs are not aligned in CMS: they are assumed to be placed at their nominal positions within their spatial resolution of about 1 cm.

Typically, the total number of hits registered along a muon track is about 40. The muon momentum is measured through its bending in the transverse plane. The radius of curvature ρ and the momentum of the muon in the plane perpendicular to the magnetic field (p_T) are related by $\rho[m] = p_T[GeV]/0.3\ B[T]$. The radius of curvature is obtained from the measurement of the muon trajectory sagitta s, after traversing a distance d in the magnetic field, using the approximate expression $\rho = d^2/8s$. An error in the sagitta measurement results in an error in the momentum measurement.

The relative error in the sagitta measurement is $\delta s/s = \delta p_T/p_T$, proportional to $\sigma(s)p_T/d^2B$, where $\sigma(s)$ is the resolution in the sagitta measurement. The relative error in the momentum increases with the muon momentum and decreases linearly with the magnetic field and quadratically with the traversed distance.

A right-handed coordinate system is used in CMS, with the origin at the nominal interaction point (IP), the X–axis pointing to the centre of the LHC ring, the Y–axis pointing up (perpendicular to the LHC plane), and the Z–axis along the anticlockwise-beam direction. The polar angle Θ is measured from the positive Z–axis and the azimuthal angle Φ is measured in the XY–plane. The pseudorapidity is a geometrical variable defined as $\eta = -\ln[\tan(\Theta/2)]$.

At 3.8 T the solenoid induces an axial force of about 10,000 ton on the endcap iron yokes in the direction of the IP. Aluminium blocks, called Z-stops, are located between the endcap disks and the barrel region, as well as between the five barrel wheels, to prevent the different structures from being crushed into each other. The positions of the Z-stops are indicated in Fig. 1. The deformation of the endcap iron disks as a result of the compression due to the magnetic forces and the resistance of the barrel Z-stops is sketched in Fig. 2.

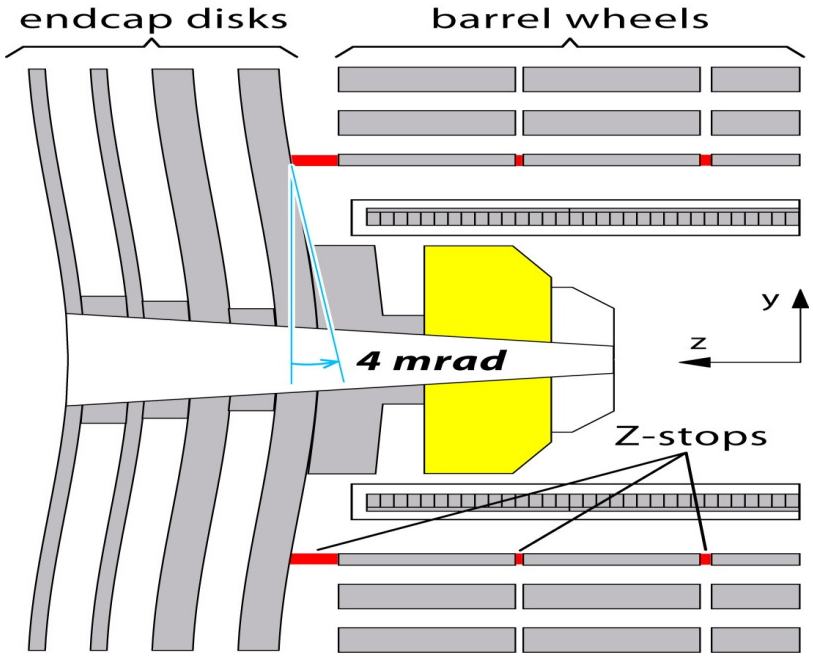

Fig. 2: *Sketch of the deformation of the endcap iron disks as a result of the compression due to the magnetic field forces and the resistance of the barrel Z-stops.*

In order to meet the muon momentum resolution requirements mentioned above, CMS is instrumented with an Alignment System organised in three basic blocks:

– The Tracker alignment system [4] measures the relative position of the various tracker modules and monitors eventual internal deformations.

– The Muon (Barrel and Endcaps) alignment system [3] monitors the relative positions among the DT and CSC muon chambers.

– The Link System connects the position of the two muon subsystems, Barrel and Endcaps to the position of the tracker body and monitors the relative movements between them.

The Link System is composed of several types of sensors supported by a series of independent reference rigid bodies which are individually calibrated and intercalibrated on special benches and measured by photogrammetry once installed in CMS. The position of the sensors define three alignment planes 60^o apart, starting at $\Phi = 15^o$. Fig. 3 a) shows one of the Φ Link alignment planes where the three alignment subsystems can be seen. Each plane contains four independent alignment quadrants where the three systems are connected. The three Φ Link planes are also depicted on Fig. 3 b), where the CMS coordinate system is also indicated. A sketch of one quadrant of a Φ Link alignment plane with its instrumentation is shown in Fig. 4.

a)

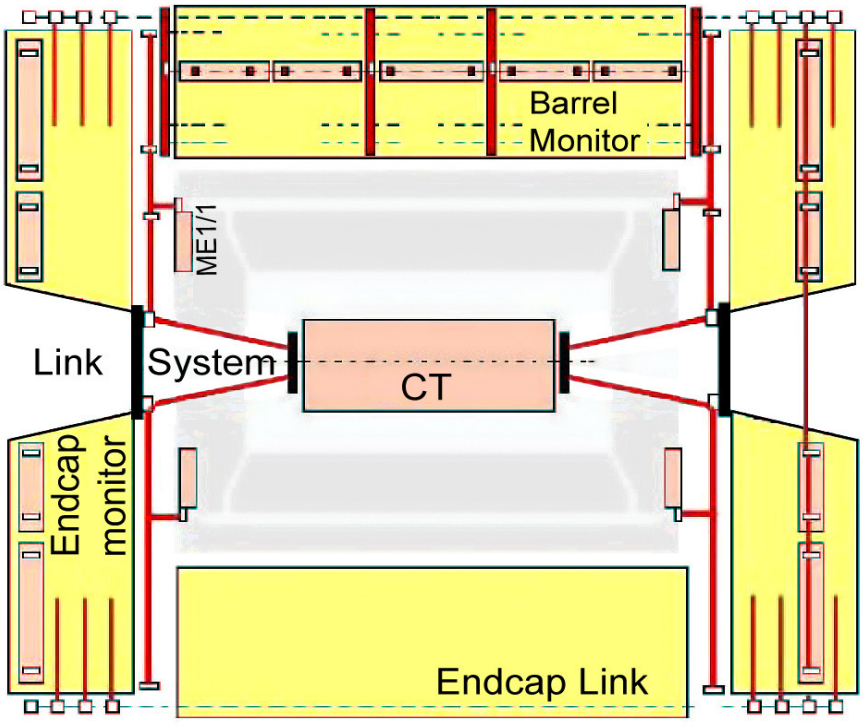

b)

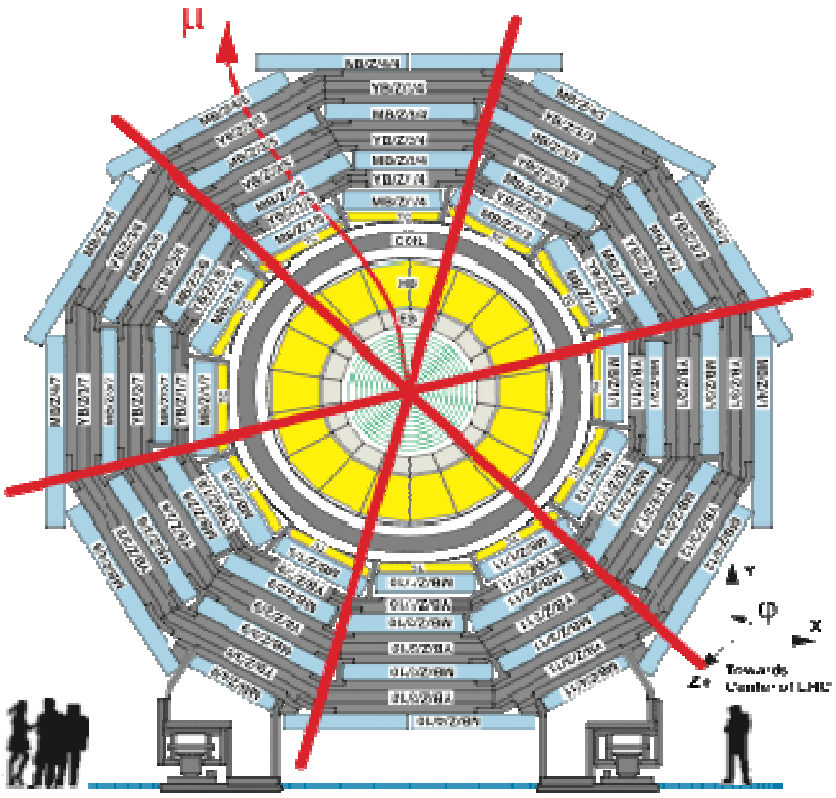

Fig. 3: *Schematic view of the Alignment System. a): one Φ alignment plane. The continuous and dotted lines show different optical paths. b): transverse view of the barrel muon detectors. The crossing lines indicate the three alignment Φ planes. The CMS coordinate system is also indicated in the figure.*

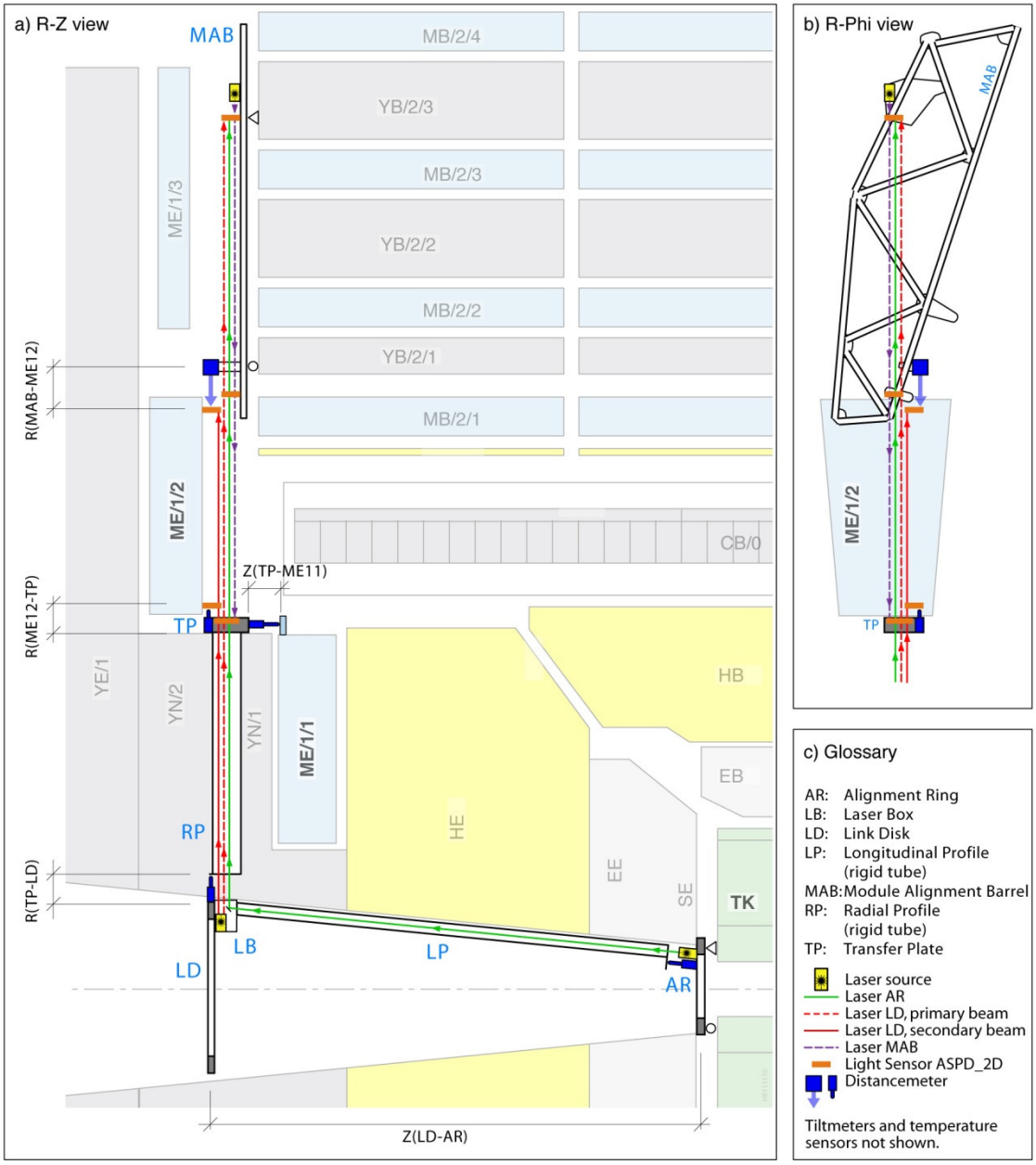

Fig. 4: *Sketch of main Link Alignment elements (not to scale) in a quadrant of a Φ plane. The distances whose variations were used to study the evolution of deformations are R(MAB–ME1/2), Z(TP–ME1/1) and Z(LD–AR). Tiltmeters and temperature sensors are not shown.*

A distributed network of Amorphous Silicon Position Sensors (ASPDs) in each quadrant is connected by laser lines. An ASPD sensor [8-10] consists of two groups of 64 silicon micro-strips 408 μm wide, with a pitch of 430 μm, oriented perpendicularly. Total active area is about 30×30 mm^2.

The measured spatial resolutions of the reconstructed light spot on the sensor active area are 5.2 ± 2.6 μm and 5.1 ± 2.4 μm for the X– and Y–sensor coordinates, respectively [10].

Each of the 12 alignment quadrants use four laser light paths, one originating at the Tracker, two at the Endcap, and one at the Barrel region as indicated in Fig. 4, resulting in 48 laser paths, 24 on each side (positive or negative Z) of the CMS detector.

All laser-source collimators are housed in rigid carbon fibre structures called Alignment Rings (ARs), Modules for the Alignment of the Barrel (MABs) and Link Disks (LDs).

The ARs are annular structures attached to the Back Disks (BDs), the outermost, uninstrumented, Tracker Endcap discs**.** The LDs, annular structures as well, are suspended from the inner diameter of the YN1 iron disks of the endcap muon spectrometer by means of aluminium tubes attached to mechanical assemblies called Transfer Plates (TPs). MABs are mounted onto the barrel yoke elements.

The laser-ASPD measurement network is complemented by electrolytic tiltmeters for angular measurements with respect to the gravity, optical and mechanical proximity sensors for short distance measurements, aluminium tubes (longitudinal and radial profiles, labelled LP and RP on Fig. 4) for long distance measurements and magnetic probes and temperature sensors (not shown in Fig. 4).

The relative distance between LD and AR structures along the CMS Z coordinate is monitored at three different Φ positions ($\pm 75^{o}$, $\pm 195^{o}$ and $\pm 315^{o}$, the sign indicating the Z side) by Sakae potentiometers [11] located at the AR in contact with targets mounted on 3610 mm long Longitudinal Profiles attached to the LD. These six variables will be the main object of the present study.

The relative Z distance between the TP and the ME/1/1 chamber is measured by a contact potentiometer installed in the TP touching a target situated on the top side of the ME/1/1 chamber (see Fig 4).

The rest of the relative distance measurements between CMS elements in a Φ quadrant monitor motions in the radial direction. The radial distance between LD and TP is the longest one monitored. It is measured using a 1977 mm long radial profile (RP in Fig. 4) instrumented with a potentiometer located in its end closest to the LD. The relative displacement between the TP and the bottom side of the ME/1/2 chamber is also monitored using a contact potentiometer. The relative radial distance between the MAB and the outer side of the ME/1/2 chamber is monitored using a non-contact proximity sensor (Omron [12]) installed at the innermost part of each MAB structure. The sensor emitting/receiving head directs a laser light and receives the reflected light to/from a reflective target located on the outer region of the ME/1/2 chamber.

The combined uncertainty in the measurement of absolute positions is estimated to be about 300 μm. It includes the uncertainty in the length of the mechanical supports, the proximity sensor resolution/precision and the mounting uncertainty. Nevertheless, relative distance measurements, which are the relevant ones for this study, are only affected by the precision of the proximity sensors, ~ 40 μm.

All the alignment structures (ARs, LDs, TPs, and MABs) are instrumented with different models of tiltmeter sensors [13] which provide direct information on any changes in their orientations (small rotations/tilts). The precision of these sensors is of the order of 40 μrad [14]. With these devices, the Link Alignment System can monitor changes in Φ (azimuthal angle, rotations around the Z-axis) and Θ (polar angle, rotations around the X−axis) of the AR, BD, LD and TP structures. Tiltmeters located in the ARs and the BDs, are sensitive to rotations (Φ) and/or bending (Θ) of the Tracker body. In the case of the tiltmeters situated in the LDs, they detect rotations and/or bending of the YN1 endcap iron disks.

For the MAB structures the only monitored angle is Φ. Fig. 5 shows a sketch of a MAB with the position of the tiltmeter attached to it. The sensor is placed in an X–Y plane in order to detect a rotation of the structure around the +Z axis. Small variations registered (μrads) with respect to the nominal Φ value of each particular MAB would indicate eventual tilts and/or deformations of the muon barrel wheels.

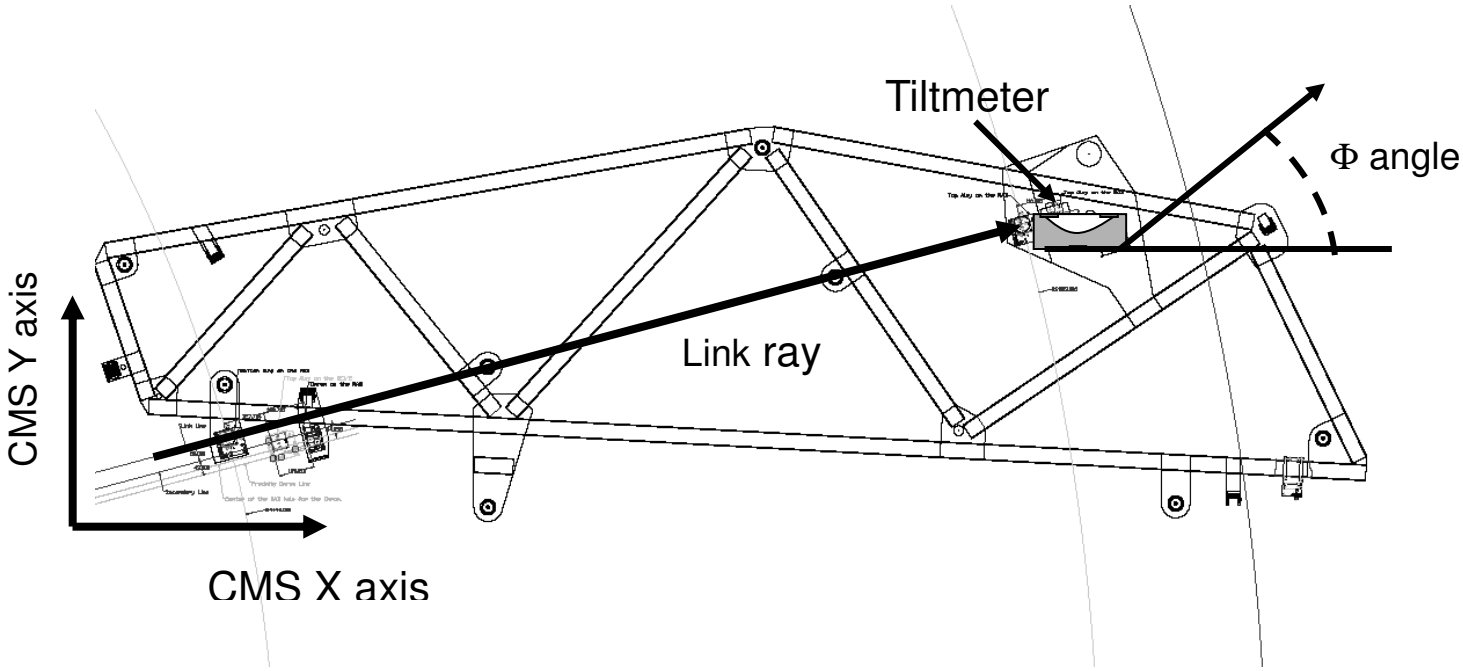

Fig. 5: A MAB structure, showing the position of the tiltmeter for Φ monitoring.

The present study focuses on the distance between the LD and its corresponding AR, called Z(LD−AR), whose variation, ΔZ(LD−AR), is monitored at three different Φ positions at both CMS Z sides (±75^o, ±195^o and ±315^o) by potentiometers located at the ARs in contact with targets mounted on 3609.691 ± 0.033 mm long Longitudinal Profiles attached to the LDs [16,17]. The reason is that these ΔZ(LD-AR) distances are the only Link Alignment surveyed variables that, according to Ref. [7], do not present full stability 24 hours after the magnetic field reaches the physics data taking value (3.8 T as from 2009). Although the longitudinal profile LP makes an angle of ~6º with the CMS Z−axis, as seen in Fig. 4, the potentiometer is placed parallel to the Z axis.

3. Magnet cycles and stability periods.

A *magnet cycle* is defined as the time elapsed between the switching on and off of the current in the coils. As said, the switch off is occasionally uncontrolled (fast dump): the current in the coils drops to 0 A in a few seconds and the magnet takes a minimum of a couple of days to restart working properly.

The lifetime of the CMS magnet is related to the number of magnet cycles. It is expected to be in the order of a few hundred cycles. Tables 1 to 6 display the magnet

cycles done during the years 2008 to 2013, respectively. These tables indicate the cycle number, the starting date, and the first link data in the cycle, the end of cycle date, the last link data in the cycle, the maximum magnetic field strength reached and the switch off conditions for that cycle (either *controlled* or *fast dump*).

Cycle nb.	Start date	Start data nb.	End date	End data nb.	B_{max} (T)	Switch off cond.
1	27/8	1	29/8	19	2.1	Controlled
2	29/8	20	8/9	41	3.0	Controlled
3	8/9	42	9/9	122	3.0	Controlled
4	7/10	123	10/10	270	3.8	Fast Dump
5	10/10	271	21/10	955	3.8	Controlled
6	21/10	956	21/10	1374	3.8	Controlled
7	21/10	1375	24/10	1427	3.8	Controlled
8	24/10	1428	6/11	1808	3.8	Fast Dump
9	6/11	1809	8/11	2341	3.8	Controlled
10	8/11	2342	12/11	2734	3.8	Controlled
11	12/11	2735	13/11	2737	3.8	Fast Dump
12	13/11	2738	14/11	2856	4.0	Fast Dump
13	14/11	2857	21/11	3203	4.0	Fast Dump

Table 1: *List of the magnet cycles during the year 2008. In cycle number 1 the maximum magnetic field reached was only 2.1 T, whereas in cycles 12 and 13, 4.0 T was reached. No new attempt to reach that field intensity was tried.*

Cycle nb.	Start date	Start data nb.	End date	End data nb.	B_{max} (T)	Switch off cond.
1	17/6	1	9/7	107	1.0	Controlled
2	10/7	108	15/7	178	1.5	Controlled
3	16/7	179	24/7	353	2.0	Controlled
4	24/7	354	24/7	359	2.0	Fast Dump
5	27/7	360	28/7	434	2.0	Controlled
6	28/7	435	29/7	546	3.8	Fast Dump
7	7/8	547	11/8	650	3.8	Controlled
8	11/8	651	18/8	1015	3.8	Controlled
9	18/8	1016	18/8	1022	3.8	Fast Dump
10	18/8	1023	30/8	3047	3.8	Controlled
11	31/8	3048	31/8	3299	3.8	Fast Dump
12	31/8	3300	23/10	3409	3.8	Fast Dump
13	26/10	3410	17/11	3861	3.8	Fast Dump
14	18/11	3862	16/12	6165	3.8	Controlled

Table 2: *List of the magnet cycles during the year 2009. In cycles numbers 1 to 5 the 3.8 T intensity is not reached. In cycle number 14 there were several 3.8 T periods before the current is switched off.*

Cycle nb.	Start date	Start data nb.	End date	End data nb.	B_{max} (T)	Switch off cond.
1	21/1	1	10/2	74	1.	Controlled
2	10/2	75	15/2	270	3.8	Controlled
3	15/2	271	25/2	568	3.8	Controlled
4	25/2	569	15/4	704	3.8	Fast Dump
5	15/4	705	26/4	956	3.8	Fast Dump
6	26/4	957	31/5	1246	3.8	Fast Dump
7	31/5	1247	19/7	1491	3.8	Controlled
8	19/7	1492	3/8	1875	3.8	Controlled
9	3/8	1876	16/8	2035	3.8	Controlled
10	16/8	2036	30/8	2375	3.8	Controlled
11	30/8	2376	2/9	2407	3.8	Fast Dump
12	2/9	2408	19/10	2762	3.8	Controlled
13	19/10	2763	8/12	3677	3.8	Fast Dump

Table 3: *List of the magnet cycles during the year 2010. In cycle number 1 the 3.8 T field is not reached. In cycles numbers 8 and 13 there were several 3.8 T periods before the current is switched off.*

Cycle nb.	Start date	Start data nb.	End date	End data nb.	B_{max} (T)	Switch off cond.
1	25/1	1	9/2	116	1.0	Controlled
2	9/2	117	28/3	623	3.8	Controlled
3	30/3	624	9/5	1184	3.8	Fast Dump
4	10/5	1185	29/6	1472	3.8	Controlled
5	29/6	1473	13/7	1569	3.8	Controlled
6	14/7	1570	6/10	1855	3.8	Controlled
7	6/10	1856	10/11	2087	3.8	Controlled
8	1/11	2088	8/11	2136	3.8	Fast Dump
9	9/11	2137	8/12	2400	3.8	Controlled

Table 4: *List of the magnet cycles during the year 2011. Notice that in cycle number 1 the 3.8 T field is not reached. In addition, during cycle number 5 there was no time (more than 24 hours) for any stability period at 3.8 T.*

Cycle nb.	Start date	Start data nb.	End date	End data nb.	B_{max} (T)	Switch off cond.
1	31/1	1	9/3	228	3.8	Fast Dump
2	9/3	229	20/6	637	3.8	Fast Dump
3	20/6	638	10/8	738	3.8	Fast Dump
4	11/8	739	22/8	764	3.8	Fast Dump
5	22/8	765	17/9	1006	3.8	Controlled
6	17/9	1007	17/9	1018	3.8	Fast Dump
7	20/9	1019	26/11	1211	3.8	Controlled
8	26/11	1212	18/12	1316	3.8	Fast Dump

Table 5: *List of the magnet cycles during the year 2012. In cycle number 2 there were several 3.8 T periods before the current is switched off.*

.

Cycle nb.	Start date	Start data nb.	End date	End data nb.	B_{max} (T)	Switch off cond.
1	9/1	1	17/2	198	3.8	Fast Dump

Table 6: *List of the magnet cycles during the year 2013.*

Link alignment data are taken either each five minutes (usually during ramping up and down in field intensity, when the ASPDs are not in operation) or twice per day (during the periods at 3.8 or 4.0 T constant field, when the ASPDs are in use). Occasionally there is no data taken during a whole day in a cycle.

The CMS magnet field intensities as a function of the Link data number along the CMS 2008 - 2013 operations are shown on Fig. 6. In total there were 58 cycles, 30 of which finished with a fast dump. Only two cycles went up to B = 4.0 T (in November 2008) and, by the end of these two cycles, it was decided that the working magnetic field for physics runs would be 3.8 T. This field intensity is enough for high momentum charged particle bending and ensures a much better stability of the current in the coils (~18164 A) than that needed for 4 T (~19140 A).

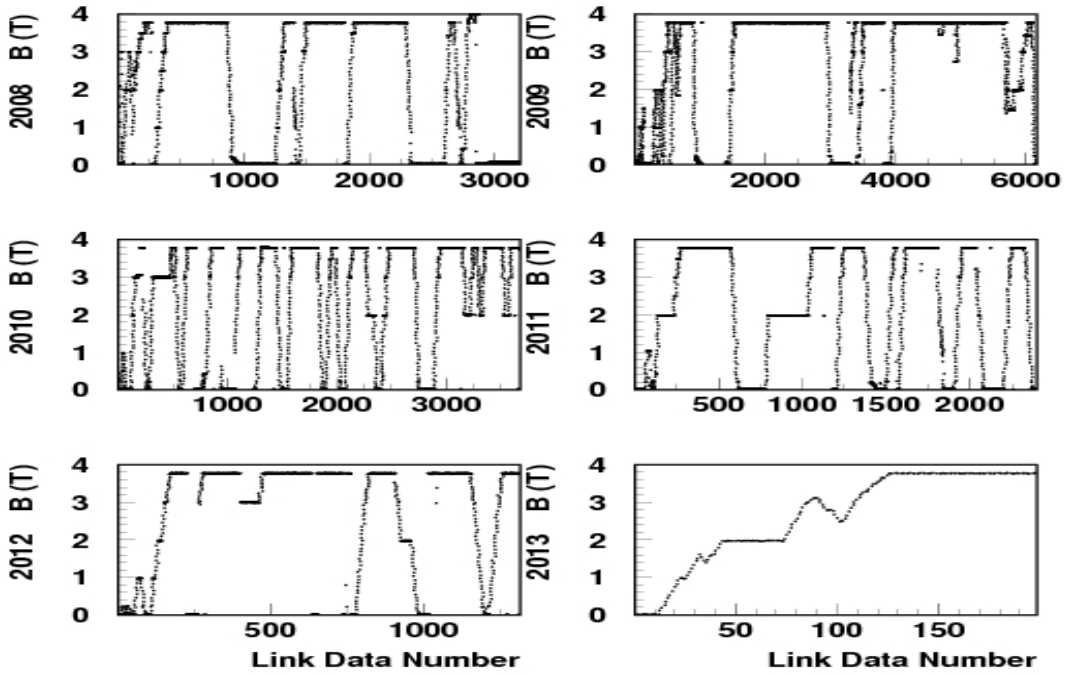

Fig. 6: *The CMS magnetic field intensities as a function of the Link data number along the CMS 2008 - 2013 operations.*

The terms “link data number” or “event number” will be used throughout this document to designate the internal sequential data number during a given Link Alignment data taking, independently of whether the run corresponds to a given year, a magnet cycle or a stability period.

As mentioned, cosmic rays, proton-proton or heavy ion collision data are taken during the magnet periods at constant B = 3.8 T or 4 T (the so-called *stability periods*). From 2008 to 2013 there were 42 stability periods, totalizing 771 days. Notice that not all the *magnet cycles* contain one *stability period*. Precise dates are given in Tables 7 to 12 for the years 2008 to 2013, respectively.

Period nb.	Start date	Start data nb.	End date	End data nb.	B (T)	Total days at B = 3.8 or 4.0 T
1	17/10	500	20/10	869	3.8	4
2	28/10	1624	29/10	1807	3.8	2
3	7/11	1943	8/11	2295	3.8	2
4	14/11	2808	14/11	2844	4.0	1

Table 7: *List of 3.8 T and 4.0 T stability periods during the CMS 2008 operation. First data considered is the one taken 24 hours after the working magnetic field intensity is reached.*

Period nb.	Start date	Start data nb.	End date	End data nb.	B (T)	Total days at B = 3.8 T
1	29/7	544	29/7	546	3.8	1
2	10/8	615	10/8	622	3.8	1
3	12/8	705	18/8	893	3.8	7
4	26/8	1623	30/8	2951	3.8	5
5	28/10	3607	5/11	3818	3.8	9
6	1/12	4027	2/12	4669	3.8	2
7	4/12	4782	4/12	4914	3.8	1
8	5/12	5037	7/12	5666	3.8	3
9	8/12	5697	9/12	5702	3.8	2
10	14/12	6083	16/12	6092	3.8	3

Table 8: *List of 3.8 T stability periods during the CMS 2009 operation. First data considered is the one taken 24 hours after the working magnetic field intensity is reached.*

Period nb.	Start date	Start data nb.	End date	End data nb.	B (T)	Total days at B = 3.8 T
1	8/3	658	14/4	704	3.8	37
2	16/4	883	23/4	947	3.8	8
3	30/4	1207	28/5	1245	3.8	29
4	3/6	1370	16/7	1418	3.8	45
5	27/7	1636	4/8	1825	3.8	9
6	3/8	1968	15/8	1990	3.8	13
7	17/8	2157	30/8	2265	3.8	14
8	3/9	2586	19/10	2708	3.8	47
9	24/10	2998	24/10	3140	3.8	1
10	25/10	3145	27/10	3154	3.8	3
11	29/10	3272	2/11	3284	3.8	5
12	4/11	3367	17/11	3517	3.8	14
13	19/11	3638	5/12	3670	3.8	17

Table 9: *List of 3.8 T stability periods during the CMS 2010 operation. First data considered is the one taken 24 hours after the working magnetic field intensity is reached.*

Period nb.	Start date	Start data nb.	End date	End data nb.	Total days at B = 3.8 T
1	11/2	338	28/3	572	46
2	16/4	1137	9/5	1182	24
3	13/5	1262	29/6	1366	47
4	15/7	1643	5/10	1806	21
5	7/10	1988	31/10	2037	25
6	13/11	2264	8/12	2327	26

Table 10: *List of 3.8 T stability periods during the CMS 2011 operation. First data considered is the one taken 24 hours after the working magnetic field intensity is reached.*

Period nb.	Start date	Start data nb.	End date	End data nb.	Total days at B = 3.8 T
1	7/3	223	8/3	226	2
2	12/3	292	10/5	401	61
3	12/5	559	18/6	634	38
4	30/6	655	9/8	736	41
5	16/8	749	21/8	762	6
6	23/8	860	15/9	907	33
7	23/9	1025	25/11	1152	64
8	30/11	1278	17/12	1314	18

Table 11: *List of 3.8 T stability periods during the CMS 2012 operation. First data considered is the one taken 24 hours after the working magnetic field intensity is reached.*

Period nb.	Start date	Start data nb.	End date	End data nb.	Total days at B = 3.8 T
1	15/1	131	17/2	198	34

Table 12: *List of 3.8 T stability periods during the CMS 2013 operation. First data considered is the one taken 24 hours after the working magnetic field intensity is reached.*

The ratio between the number of *stability days* and the number of *operation days* (days in which the coils receive current) in a given year may give an idea of the *efficiency of the operation* over that year. Table 13 displays this information for the period 2008 – 2013. As seen in column 4, the efficiency grows (but for the year 2011) with the expertise, from 10% in 2008 to 85% in 2013. In all, from a total of 1272 days of CMS underground operation, 771 where stable days for data taking, that corresponds to an average CMS operating efficiency of 60.6%. The definition used here has nothing to do with the one referring to the ratio between the luminosity delivered by LHC and the one recorded by CMS.

Year	Days of operation	Stability Days	Efficiency (%)
2008	87	9	10.3
2009	183	34	18.6
2010	322	242	75.2
2011	318	189	59.4
2012	322	263	81.7
2013	40	34	85.0
Total	1272	771	60.6

Table 13: *Efficiency (as defined in the text) of the operation per year and for the whole 2008 to 2013 CMS operation.*

Notice that a stability period, in the present study, starts 24 hours after the working magnetic field intensity is reached. At that moment, and according to Ref. [7], the CMS Experiment is in *structural equilibrium*: any further eventual displacement in any direction (axial or radial) will remain within the distance sensors resolution: ~ 40 μm and any rotation/tilt within the tiltmeters resolution: ~ 40 μrad.

However and as also remarked in Ref. [7], an apparent *accordion* motion was still detectable, during the stability periods, in the axial distance between the Link Disks and the corresponding Alignment Rings at the six equipped angles. In that study, those distances were the only ones showing variations larger than the resolution of the corresponding short distance measuring sensors (40 μm) and, as said, will constitute the main object of the present study.

4. Results of the measurements of the Z(LD-AR) distances during the Magnet Cycles along the 2008 – 2013 CMS operations.

The axial distance Z, between the LD and the AR in each of the CMS Z-sides is measured by means of a long aluminium profile (LP in Fig. 4) and a short distance measurement potentiometer. There are three LPs per Z-side. The LPs are attached to the corresponding LD and sustained in its middle length from the HE calorimeter.

A target installed at the end of the LP is touched by the rod of a Sakae potentiometer located in the AR. The quantity readout by the Link System is a resistance proportional to the rod position. When the LDs move towards their corresponding ARs by the action of the magnetic forces when passing from 0 T to B_{max}, the targets on the LPs push the rods of the potentiometers. On the contrary, when the current in the coil goes down to 0 A the reading of the sensors indicate how much the LDs move apart from their corresponding ARs.

Figs. 7 to 12 show for the 2008 to 2013 operations, respectively, the measured Z (LD−AR) distance as a function of the Link Data Number showing the motions commented above at the six Φ angles (three per Z side). As seen from the figures the LDs approach the ARs by around 15 mm due to the magnetic field forces when B reaches B_{max}. When back to B = 0 T the LDs separate from their corresponding ARs by a similar amount to recover the initial positions.

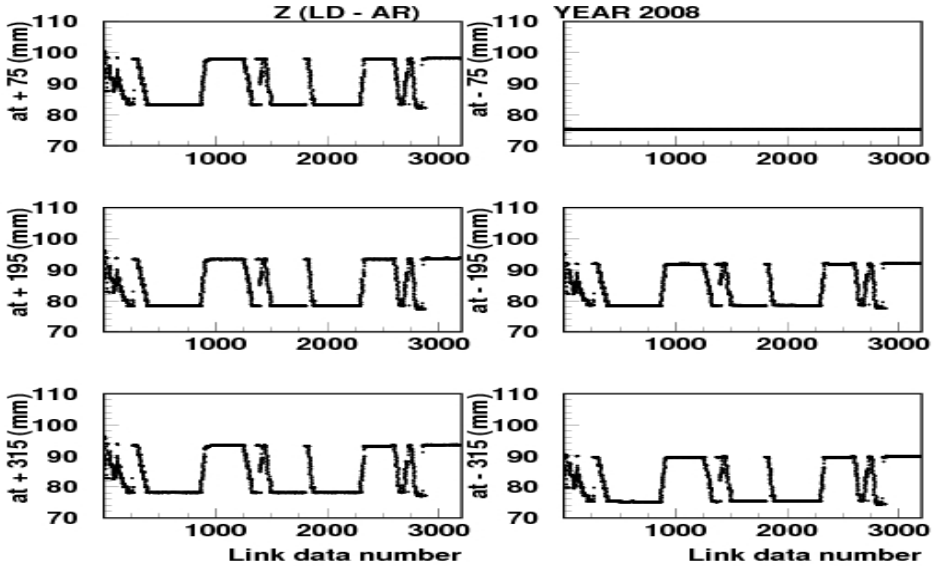

Fig. 7: *In the vertical axis, the Z (LD-AR) distance during the year 2008 monitored by the Sakae potentiometers at six Φ quadrants (± 75°, ± 195° and ± 315°, the sign refers to the CMS Z side) as a function of the link system data number. The sensor at −75° was out of order during the full data taking. There were 13 magnet cycles (see Table 1).*

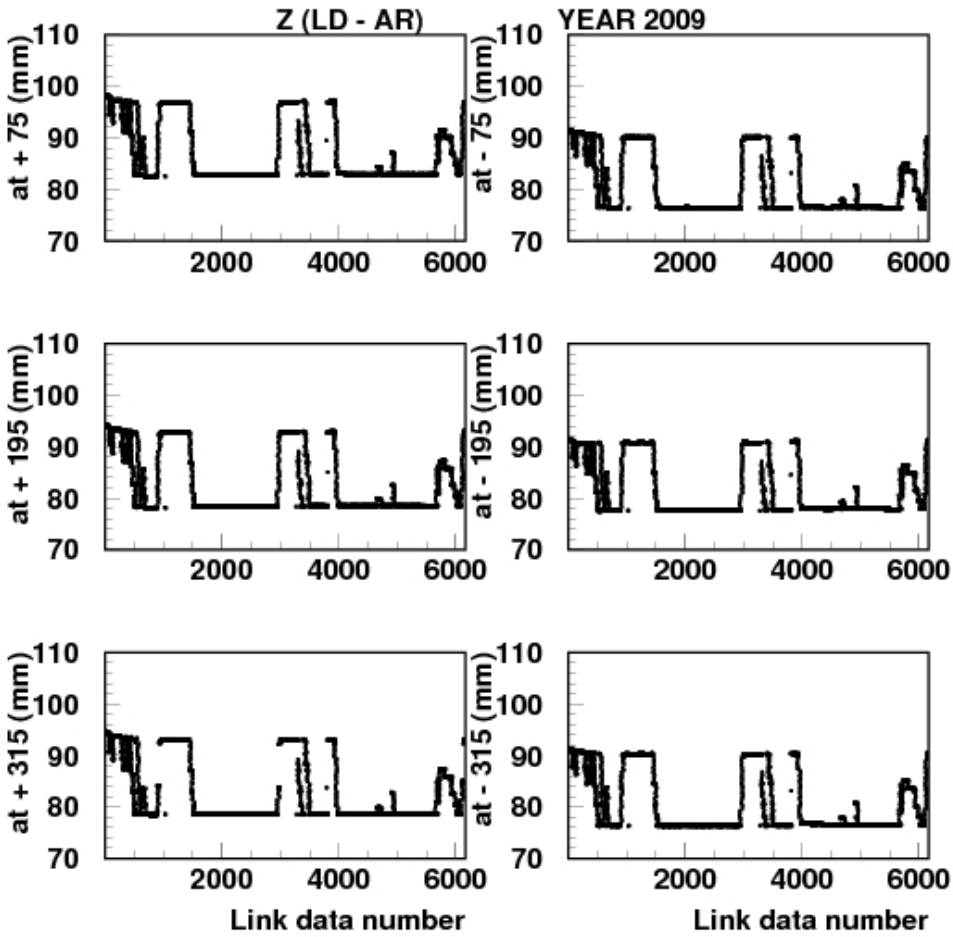

Fig. 8: *In the vertical axis, the Z (LD-AR) distance during the year 2009, monitored by the Sakae potentiometers at six Φ quadrants (± 75°, ± 195° and ± 315°, the sign refers to the CMS Z side) as a function of the link data number. There were 14 magnet cycles (see Table 2).*

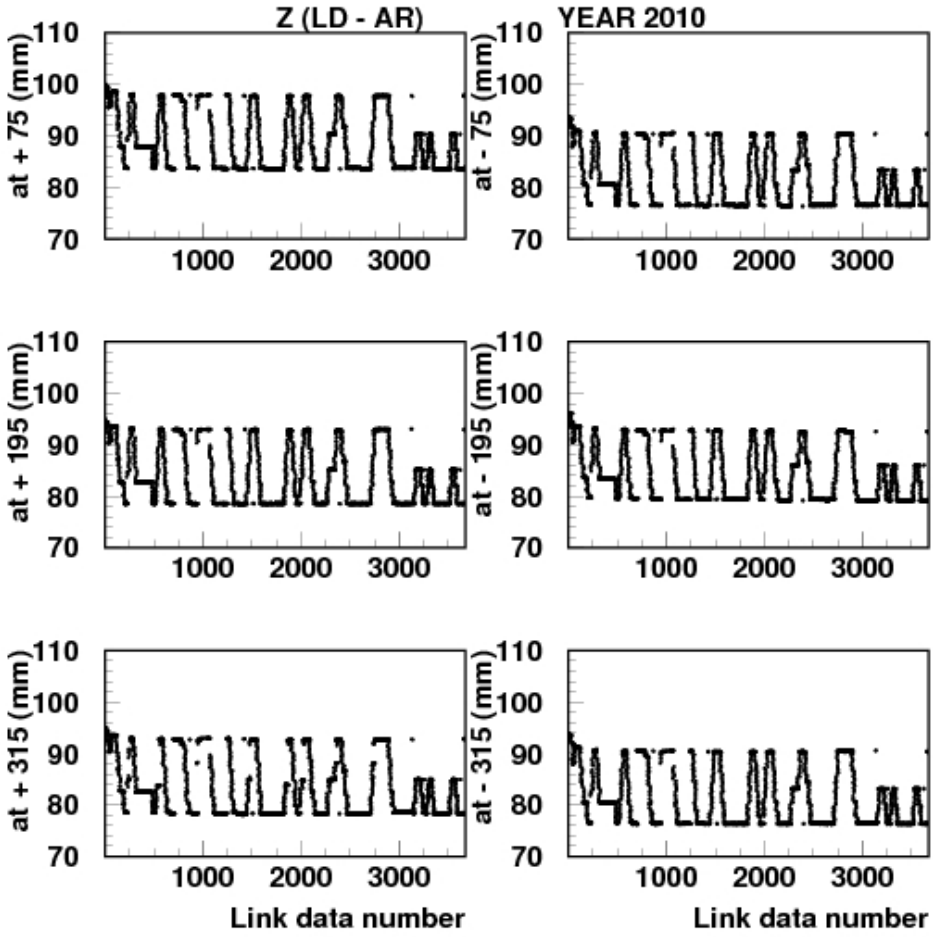

Fig. 9: *In the vertical axis, the Z (LD-AR) distance during the year 2010, monitored by the Sakae potentiometers at six Φ quadrants (± 75^o, ± 195^o and ± 315^o, the sign refers to the CMS Z side) as a function of the link data number. There were 13 magnet cycles (see Table 3).*

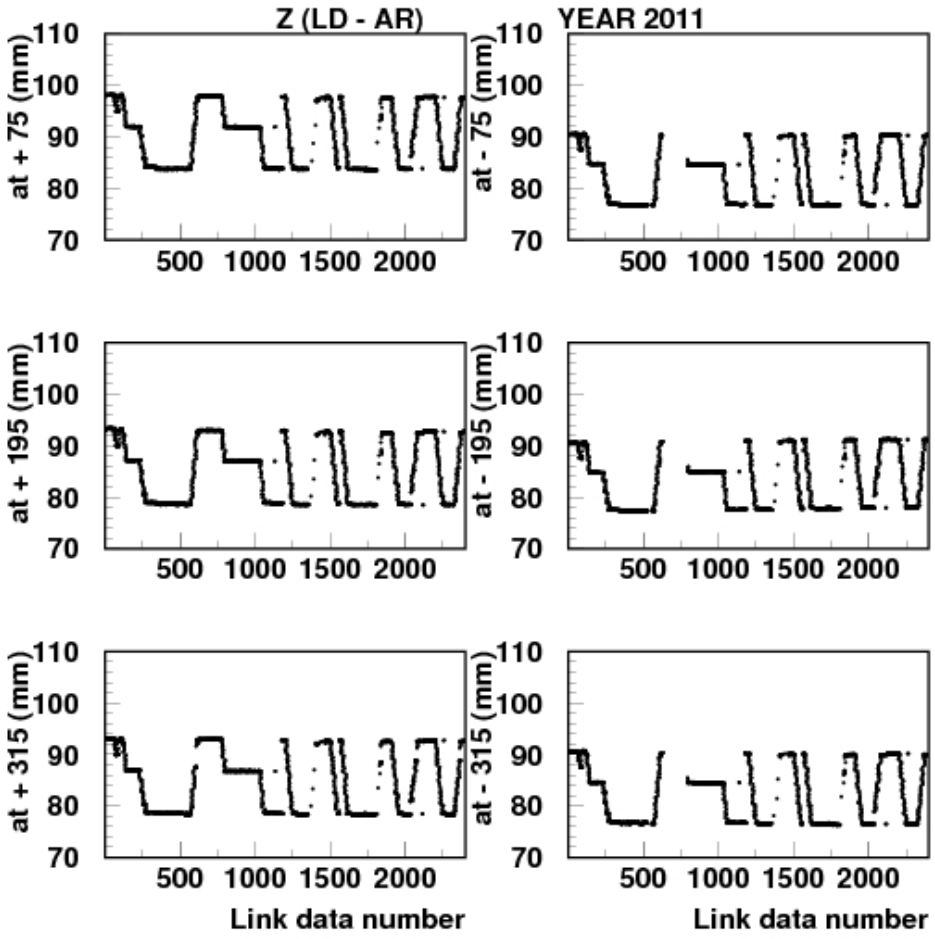

Fig. 10: *In the vertical axis, the Z (LD-AR) distance during the year 2011, monitored by the Sakae potentiometers at six Φ quadrants (± 75^o, ± 195^o and ± 315^o, the sign refers to the CMS Z side) as a function of the link data number. There were 9 magnet cycles (see Table 4).*

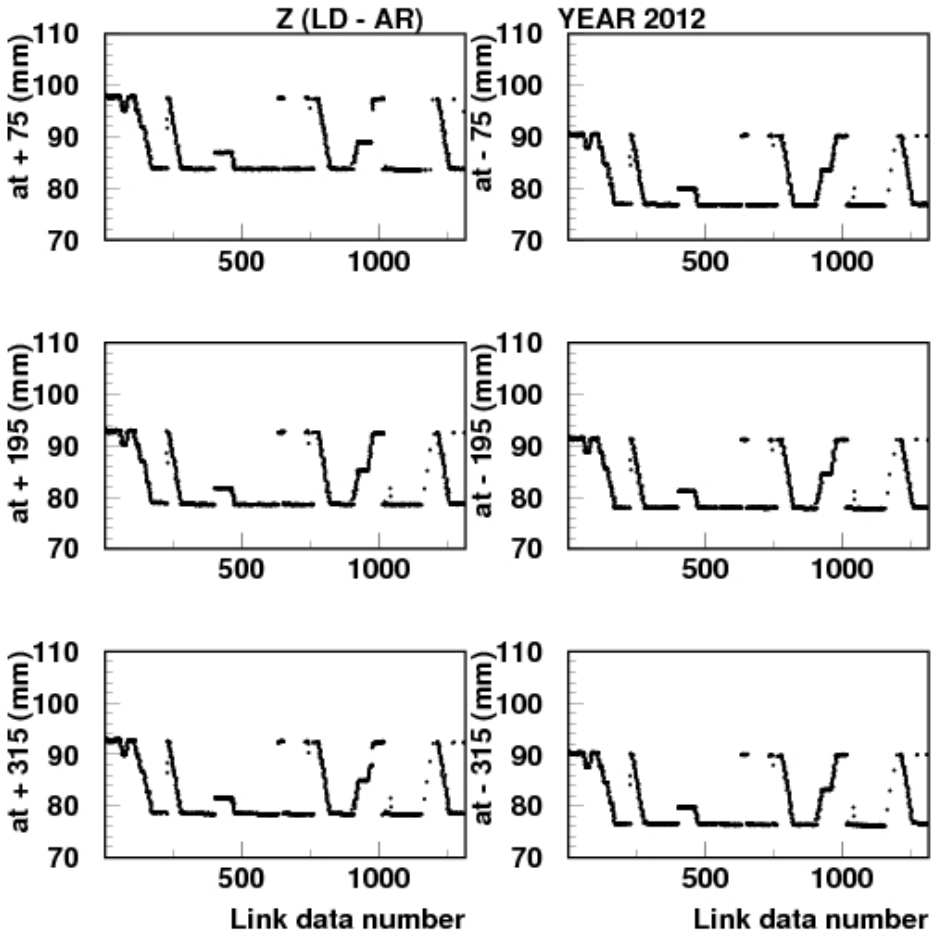

Fig. 11: *In the vertical axis, the Z (LD-AR) distance during the year 2012, monitored by the Sakae potentiometers at six Φ quadrants (± 75^o, ± 195^o and ± 315^o, the sign refers to the CMS Z side) as a function of the link data number. There were 8 magnet cycles (see Table 5).*

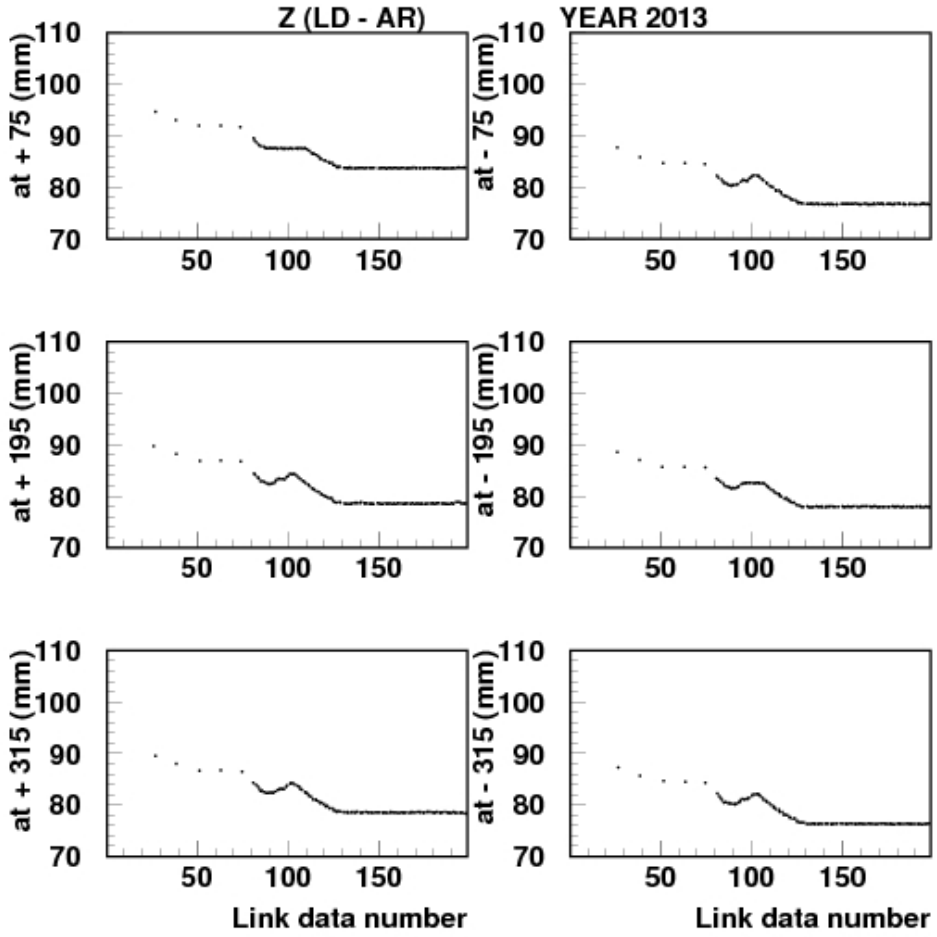

Fig. 12: *In the vertical axis, the Z (LD−AR) distance during the year 2013, monitored by the Sakae potentiometers at six Φ quadrants (± 75°, ± 195° and ± 315°, the sign refers to the CMS Z side) as a function of the link data number. In the year 2013 there was only one Magnet Cycle (see Tables 6) lasting 40 days with a unique Stability Period of 34 days.*

The monitored ΔZ of LD to AR relative distance is defined as ΔZ(LD−AR) = Z $(LD-AR)_{data\text{-}number}$ − Z$(LD-AR)_{initial}$, where the initial Z(LD−AR) value is the distance recorded at B = 0 T (at the six Φ positions), before ramping up to the desired B_{max} (4 or 3.8 T). Fig. 13 shows, as an illustration, ΔZ (LD−AR) at the Φ = 75° quadrant in the CMS +Z side during the first magnet cycle in 2012 (see Table 5), where the top figure is the histogram of the 228 ΔZ data points, with a maximum approaching motion registered of 14.99 mm; the middle figure gives ΔZ as a function of the Link Data Number **(**in the last two data points, B = 0 T and LD returns around its initial position); and the bottom figure shows ΔZ as a function of the magnetic field intensity showing the expected quadratic behaviour [7].

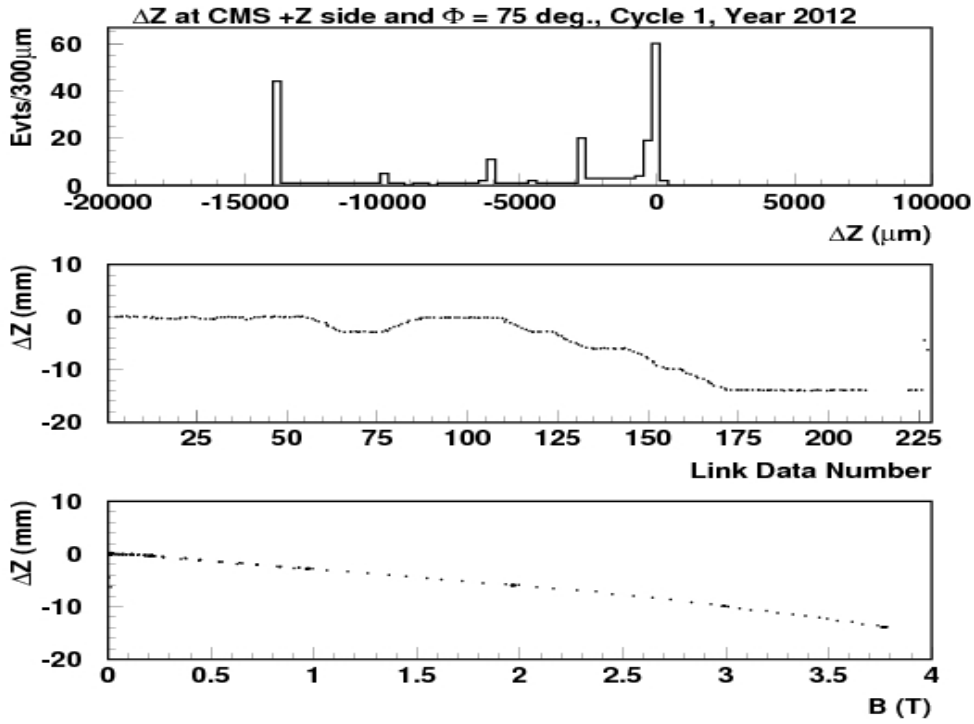

Fig. 13: *ΔZ (LD-AR) monitored by the Sakae potentiometer at the Φ = +75° quadrant, the sign refers to the CMS Z, during the first magnet cycle in 2012 (see Table 5). Top: histogram of data points. The maximum motion registered is -14.99 mm. Middle: ΔZ as a function of the Link Data Number. By the last data B = 0 T and LD returns to its initial position. Bottom: ΔZ as a function of the magnetic field intensity showing the expected quadratic behaviour.*

As pointed out in Ref [7] the relative LD−AR distance follows a quadratic law with B that, although quite similar between different magnet cycles, is far from being identical for all of them. To illustrate this point we show in Tables 14 to 19, for the years 2008 to 2013, respectively, the following quantities: the reached B_{max} before the coil current was switched off (column 1), the number of Magnet Cycles reaching this B_{max} during the given year (column 2), and the average of the maximum approach of the LD to its corresponding AR recorded at the six Φ positions (columns 3 to 8) over the cycles in column 2. It is clear that for the same magnetic field intensity the average maximum motions of LDs towards their corresponding ARs are different, well beyond one standard deviation, among the various years of observations.

B_{max} (T)	#Cycles	+75°	+195°	+315°	−75°	−195°	−315°
2.1	1	8.92± 0.04	9.21±0.04	9.21±0.04	---	9.50±0.04	6.81±0.04
3.0	1	11.05± 0.04	11.35±0.04	11.64±0.04	---	9.81±0.04	10.76±0.04
3.8	8	14.85± 0.11	15.15±0.11	15.25±0.23	---	13.52±0.15	14.34±0.20
4.0	2	15.86± 0.15	16.32±0.02	16.32±0.02	---	14.47±0.01	15.41±0.01

Table 14: *For the year 2008. Column 1: reached B_{max}; column 2: number of cycles with that B_{max}; columns 3 to 8: average ΔZ (LD-AR) values at the given Φ quarter (the sign corresponds to the CMS Z side). All measurements are given in mm. The errors are the standard deviation plus the systematic (±0.04 mm) in quadrature. The potentiometer at −75° was out of order all the year.*

B_{max} (T)	#Cycles	+75°	+195°	+315°	−75°	−195°	−315°
1.0	1	3.50±0.04	3.73±0.04	3.78±0.04	3.44±0.04	3.44±0.04	3.44±0.04
1.5	1	4.94±0.04	4.94±0.04	4.94±0.04	4.60±0.04	4.60±0.04	4.60±0.04
2.0	3	6.17±0.01	6.17±0.01	6.27±0.16	6.17±0.01	6.17±0.01	6.17±0.01
3.8	8	14.28±0.10	14.58±0.10	14.60±0.15	13.90±0.18	13.35±0.05	14.03±0.14

Table 15: *For the year 2009. Column 1: reached B_{max}; column 2: number of cycles with that B_{max}; columns 3 to 8: average ΔZ (LD-AR) values at the given Φ quarter (the sign corresponds to the CMS Z side). All measurements are given in mm. The errors are the standard deviation plus the systematic (±0.04 mm) in quadrature.*

B_{max} (T)	#Cycles	+75°	+195°	+315°	−75°	−195°	−315°
1.0	1	4.61±0.04	4.61±0.04	4.61±0.04	5.88±0.04	5.70±0.04	5.59±0.04
3.8	12	14.25±0.12	14.50±0.12	14.55±0.15	13.96±0.14	13.57±0.09	14.26±0.09

Table 16: *For the year 2010. Column 1: reached B_{max}; column 2: number of cycles with that B_{max}; columns 3 to 8: average ΔZ (LD-AR) values at the given Φ quarter (the sign corresponds to the CMS Z side). All measurements are given in mm. The errors are the standard deviation plus the systematic (±0.04 mm) in quadrature.*

B_{max} (T)	#Cycles	+75°	+195°	+315°	−75°	−195°	−315°
1.0	1	3.14±0.04	3.14±0.04	3.14±0.04	2.82±0.04	2.82±0.04	2.82±0.04
3.8	8	14.25±0.10	14.53±0.11	14.54±0.11	13.73±0.09	13.34±0.03	13.77±0.16

Table 17: *For the year 2011. Column 1: reached B_{max}; column 2: number of cycles with that B_{max}; columns 3 to 8: average ΔZ (LD-AR) values at the given Φ quarter (the sign corresponds to the CMS Z side). All measurements are given in mm. The errors are the standard deviation plus the systematic (±0.04 mm) in quadrature.*

B_{max} (T)	#Cycles	+75°	+195°	+315°	−75°	−195°	−315°
3.8	8	13.85±0.14	14.02±0.24	14.12±0.14	13.68±0.07	13.47±0.13	13.71±0.12

Table 18: *For the year 2012. Column 1: reached B_{max}; column 2: number of cycles with that B_{max}; columns 3 to 8: average ΔZ (LD-AR) values at the given Φ quarter (the sign corresponds to the CMS Z side). All measurements are given in mm. The errors are the standard deviation plus the systematic (±0.04 mm) in quadrature.*

B_{max} (T)	#Cycles	+75°	+195°	+315°	−75°	−195°	−315°
3.8	1	11.30±0.04	---	14.23±0.04	13.66±0.04	13.66±0.04	13.95±0.04

Table 19: *For the year 2013. Column 1: reached B_{max}; column 2: number of cycles with that B_{max}; columns 3 to 8: average ΔZ (LD-AR) values at the given Φ quarter (the sign corresponds to the CMS Z side). All measurements are given in mm. The errors are the standard deviation plus the systematic (±0.04 mm) in quadrature.*

In addition to the fact that same magnetic field forces produce different motion amplitudes in the approaching of the LDs to their corresponding ARs, Tables 14 to 19 also show something systematic: the axial motions in the +Z CMS side are about 4.8 % larger than in the −Z side for all 6 monitored years, without any clear explanation.

5. Study of the ΔZ(LD−AR) measurements during the Stability Periods along the 2008 – 2013 CMS operations.

As said, from the analysis of the Link Data from the years 2008 to 2010 it was observed [7] that 24 hours after the magnet reaches its working field, CMS attains its mechanical equilibrium: any further eventual displacement in any direction (axial or radial) will remain within the distance sensors resolution: 40 μm and any rotation within the tiltmeters resolution: 40 μrad. These elapsed times are called Stability Periods (SPs). As seen from Tables 7 to 12, there were 41 stability periods at 3.8 T and 1 at 4.0 T along the years 2008 to 2013.

This mechanical equilibrium, however, does not seem to apply to the ΔZ(LD−AR) relative distance, the magnitude most affected by the magnetic field forces. The ΔZ distributions at the six Φ positions were therefore studied in the 42 SPs. The quantity ΔZ is defined as $\Delta Z(LD-AR) = Z\ (LD-AR)_{data\text{-}number} - Z(LD-AR)_{initial}$ where, now, the initial Z(LD−AR) value corresponds to the first data taken, at each of the six Φ positions, 24 hours after B_{max} is reached (considered here as the starting point of full CMS mechanical equilibrium in the given period).

For all 42 Stability Periods in the six monitored years of operation, Fig.14 summarizes the ΔZ (LD−AR) relative distances monitored by the LP−Sakae potentiometer sets. At each SP the two extreme monitored values registered are plotted: the black dots represent the maximum LD−AR approach (negative values) and the open circles correspond to the maximum LD−AR separation in the apparent “accordion” motion. In most of the cases either the approach or the separation (or even both) exceed the 40 μm resolution of the short distance measurement devices.

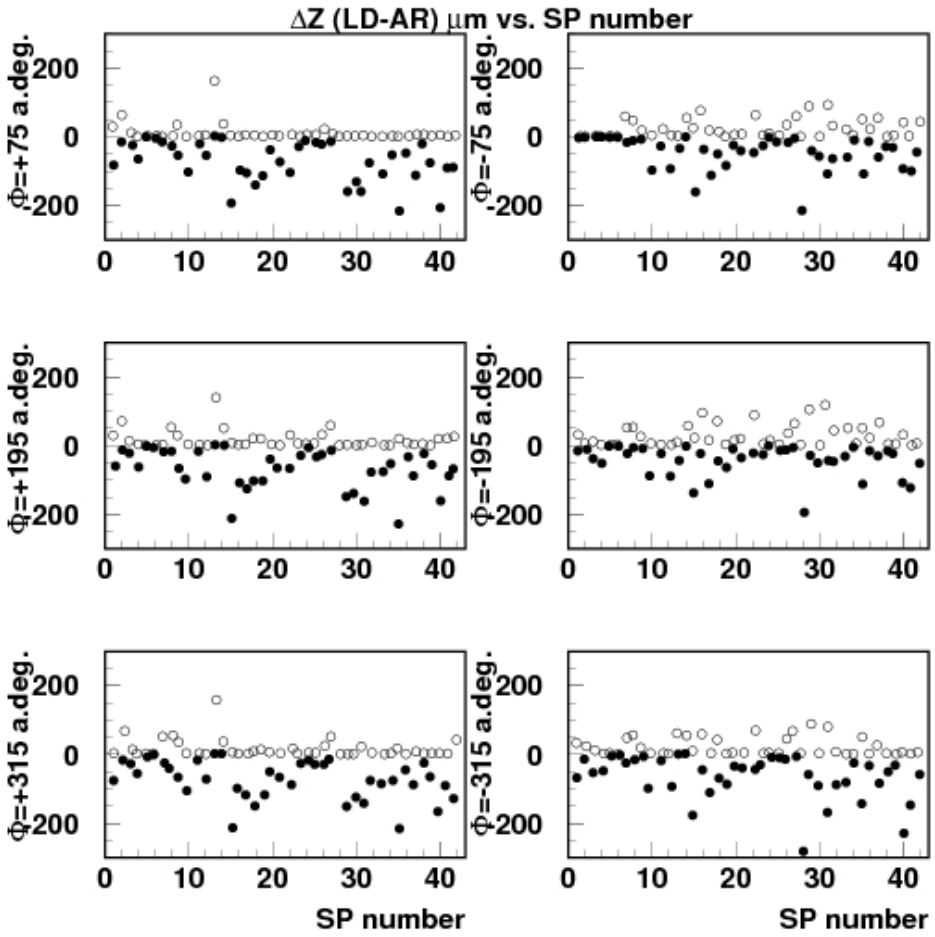

Fig.14: *ΔZ (LD-AR) monitored by the Sakae potentiometers during the 42 Stability Periods along the 2008 to 2013 CMS years of operation. ΔZ(LD-AR) = Z (LD-AR)$_{data-number}$ – Z(LD-AR)$_{initial}$, where the initial Z(LD-AR) values are read out at B = B$_{max}$ (3.8 or 4 T) at the six Φ positions corresponding to the first data taken 24 hours after B$_{max}$ is reached. For each SP the two extreme monitored values registered are shown: the black dots represent the maximum LD-AR approach (negative values) and the open circles correspond to the maximum LD-AR separation in the apparent "accordion" motion.*

Fig. 15 is an illustration of the monitored ΔZ(LD−AR) during some SPs (taken at random) along the six investigated years. For a given SP during a certain year of operation, the measured ΔZ(LD−AR) value is plotted as a function of the Link Data Number. For the years 2008 and 2009 a measurement is recorded every five minutes. In all other cases there is a maximum of two data points per SP day. The distributions are far from being constant or smooth over time, and motions surpassing ±40 μm are clearly seen. We will use these same six, Operation Year – Stability Period (OY−SP), data sets for further illustrations in what follows.

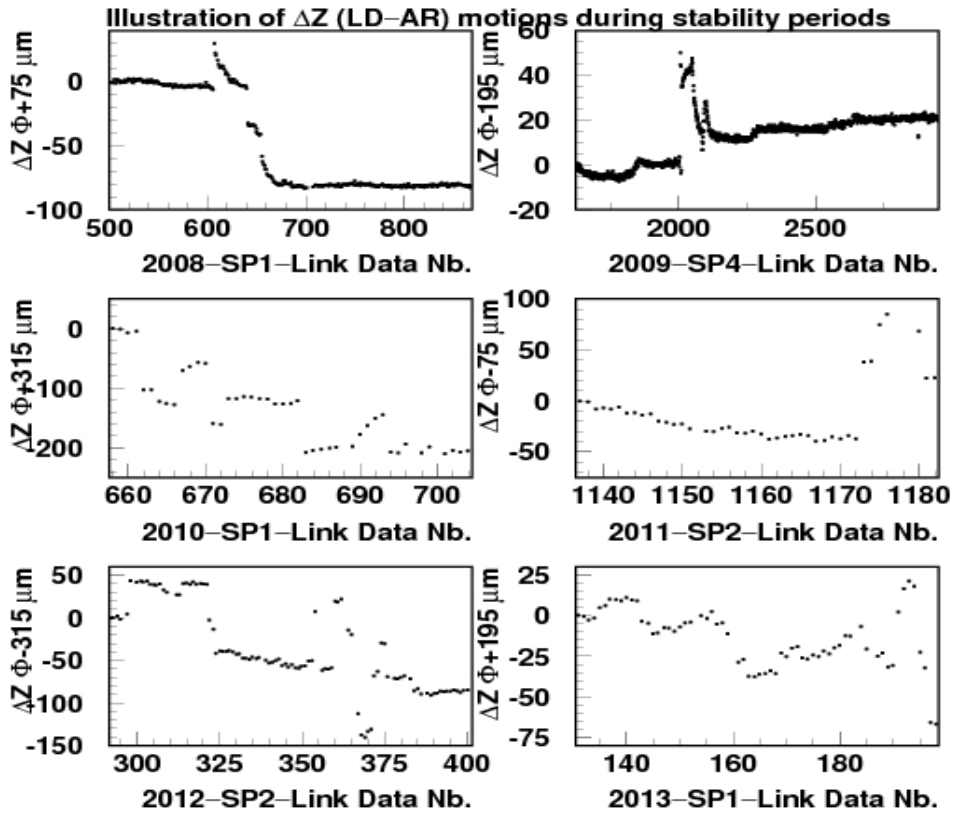

Fig. 15: *ΔZ(LD-AR) distance measurements, in microns, for the indicated Φ quadrant (sign refers to + or – Z CMS side) as a function of the Link Data Number internal to the indicated Stability Period for the mentioned year.*

When the current in the coil remains stable, as is the case during the SPs, there is no motion due to any change in magnetic forces. Under these circumstances the motions seen in Figs. 14 and 15 correspond either to unknown but real small mechanical displacements of the muon endcap system towards to or away from the Tracker, or to something else that has to be determined. One possibility is temperature changes.

The length of the LPs, measured at the Alignment Laboratory in the ISRs before mounting in CMS, was on average L = 3609.691 ± 0.033 mm referred to a temperature of 20 ^{o}C [16, 17]. Being made of aluminium, a change in the temperature of the profile by an amount ΔT (^{o}C) = $T_{measured}$ (^{o}C) – 20 (^{o}C) will result in a change of the length of the order of ΔL (μm) = 24 (μm m^{-1} ^{o}C^{-1}) × 3.609691 (m) × ΔT (^{o}C). In that case the Z(LD−AR) distances would have to be corrected by the change in the LP length, but this is not necessarily the case for the relative ΔZ(LD−AR) distance. The relative ΔZ(LD−AR) distance measurement will be affected by temperature changes only in the case that they occur during the data taking. This is investigated in what follows.

5.1 Temperature monitoring in the LDs to ARs CMS volumes.

PT100 temperature probes monitor the temperature in the neighbourhoods of the LPs. At the Link Disks there are probes at the six Φ sextants (15, 75, 135, 195, 255 and 315 arc. deg. respectively) at both +Z and –Z CMS sides. At the Alignment Rings there are two probes at Φ = 90 and 270 arc. deg. respectively.

The temperature in the proximities of the Link Disks (TLD at + or – Z CMS side) associated to a recorded Link Data is defined as the average value of the six corresponding PT100 probes. The one in the proximities of the Alignment Rings (TAR+ or TAR−) is taken as the average of the two corresponding PT100 probes. The temperature in the air volume between the Link Disks and the Alignment Rings associated to a recorded Link Alignment Data is calculated as the mean value of TLD and TAR at the considered Z side (represented by T+ and T−).

The calculated mean value of the temperature in the neighbourhoods of the aluminium profiles for the SPs used for the ΔZ(LD−AR) monitoring in Fig. 15 are displayed in Fig. 16 as a function of the Link Data Number. The plotted mean temperature values correspond to the same CMS Z sides as the Φ angles in Fig. 15. Correlations between bumps in one figure and dips in the other (and vice versa) can be appreciated.

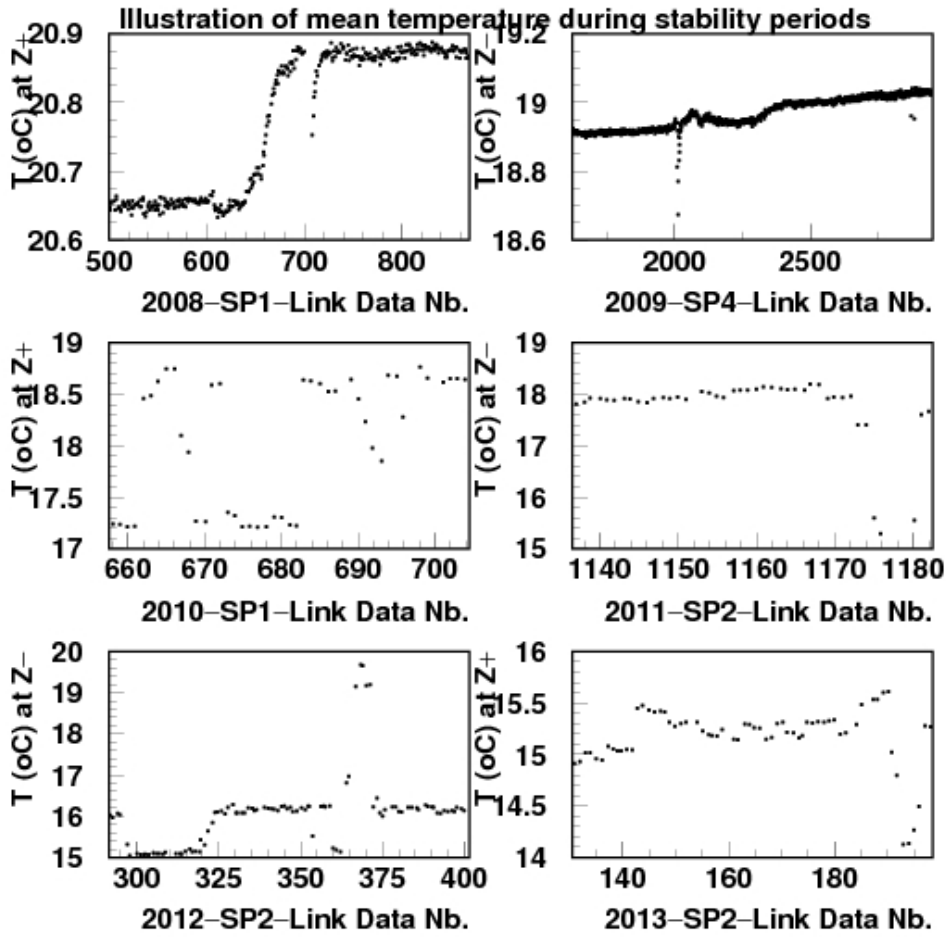

Fig 16: *Averaged temperature, in ^{o}C, in the neighbourhoods of the aluminium profiles for the indicated CMS Z side (sign refers to the side) as a function of the Link Data Number during the mentioned OperationYear−StabilityPeriod data set. There is a one to one correspondence with the Φ quadrants in Fig. 15.*

The numerical values of the monitored temperatures in the Link Disks – Alignment Rings volumes are given in Table 20 for the years and the Stability Periods used in the text and in Fig. 16 as examples. Columns 2 to 4 correspond to the Z+ CMS side. Column 2 gives the average temperature measured at the Link Disk (over six PT100

sensors); column 3 is the average (over two PT100 sensors) at the Alignment Ring. Column 4 (T+) gives the average value of the measurements taken at the Link Disk and the Alignment Ring that will be assumed to be the Longitudinal Profiles temperature. Columns 5 to 7 are the corresponding values measured at the Z− CMS side. All measurements are given in ^{o}C and the errors are the RMS of the corresponding distributions. A PT100 sensor has a resolution better than 0.01 ^{o}C.

Year_SPi	TLD +	TAR +	T +	TLD −	TAR −	T −
2008_SP1	21.69±0.16	19.85±0.06	20.77±0.11	21.62±0.13	20.46±0.04	21.04±0.08
2009_SP4	20.10±0.13	16.58±0.06	18.34±0.05	20.20±0.12	17.74±0.05	18.97±0.04
2010_SP1	20.76±0.05	15.33±1.25	18.04±0.63	20.81±0.04	18.25±1.16	19.53±0.59
2011_SP2	19.35±0.06	14.98±1.49	17.17±0.76	19.43±0.06	16.09±1.28	17.76±0.66
2012_SP2	19.22±0.14	11.55±1.97	15.38±1.00	19.21±0.13	12.91±1.78	16.06±0.90
2013_SP1	19.20±0.30	11.10±0.50	15.20±0.30	19.30±0.40	12.50±0.50	15.90±0.30

Table 20: *For the years and Stability Periods used in the text as examples. Columns 2 to 4 correspond to the Z+ CMS side. Column 2 gives the average temperature measured at the Link Disk with six PT100 sensors, column 3 is the average (over two PT100 sensors) at the Alignment Rings. Column 4 (T+) gives the average value of the measurements taken at the Link Disk and the Alignment Ring, representing the Longitudinal Profiles temperature. Columns 5 to 7 are the corresponding values measured at the Z− CMS side. All measurements are given in ^{o}C. The errors are the RMS of the corresponding distribution. A PT100 sensor has a resolution better than 0.01 ^{o}C.*

A first observation of Table 20 shows that the temperatures at the Alignment Rings (TAR, in both Z CMS sides) are much smaller (given the RMS values) than those at the Link Disks (TLD) neighborhoods most probably due to Tracker operations.

The second observation is that the average temperature (T), in the LD−AR volume (the one to be assigned to the aluminum Longitudinal Profiles, LPs), is slightly higher (~1^{o}C) at the CMS Z− side than at the Z+ side.

A detailed representation of the data in Table 20 for the six considered OY−SP data sets are shown in Figs. 17 to 22, where the monitored temperature in each of them is plotted as a function of the Link Data Number, respectively. The left column of drawings in a given figure corresponds to the CMS Z+ side. The three plots represent, respectively, the temperature measured near the Link Disk (TLD, averaged over 6 PT100 sensors), near the Alignment Ring (TAR, averaged over 2 PT100 sensors) and the assumed LP temperature, T = (TLD + TAR)/2, in the air volume around the Long aluminum Profiles joining the Link Disk to its corresponding Alignment Ring. The three drawings of the right column correspond to the recorded data at the CMS Z−side.

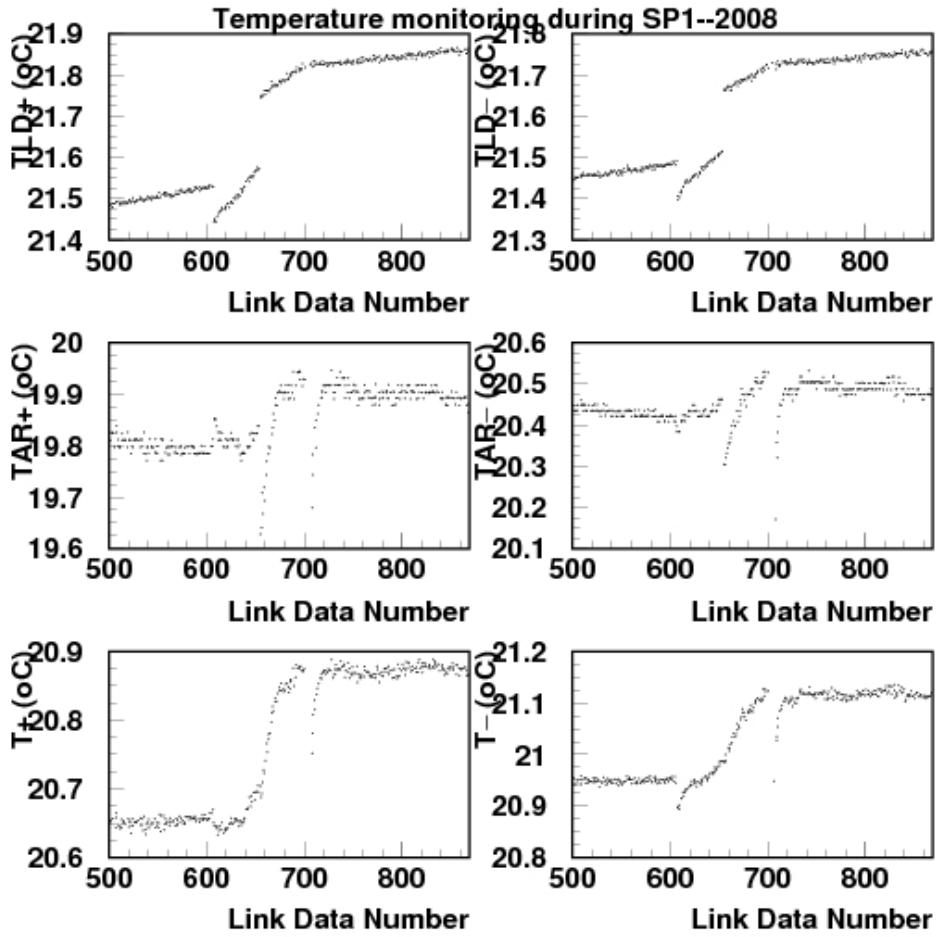

Fig 17: *Monitoring of the temperature during the SP1 in year 2008 as a function of the Link Data Number. Data are recorded every five minutes. Left column corresponds to CMS Z+ side, the three plots represent the temperature measured near the Link Disk (6 PT100 sensors), the Alignment Ring (2 PT100 sensors) and the assumed temperature, T = (TLD + TAR)/2, in the air volume around the Long Profiles joining the Link Disk to its corresponding Alignment Ring. Right column are the recorded data at the Z− side.*

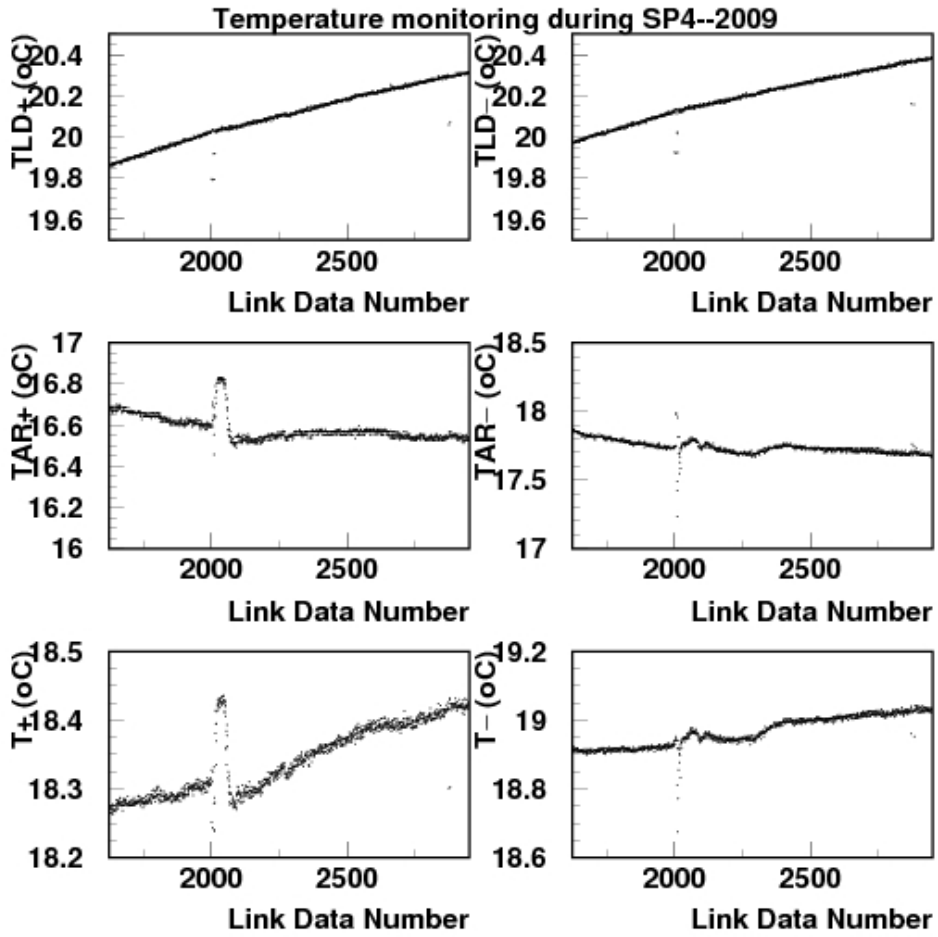

Fig 18: *Monitoring of the temperature during the SP4 in year 2009 as a function of the Link Data Number. Data are recorded every five minutes. Left column corresponds to CMS Z+ side, the three plots represent the temperature measured near the Link Disk (6 PT100 sensors), the Alignment Ring (2 PT100 sensors) and the assumed temperature, T = (TLD + TAR)/2, in the air volume around the Long Profiles joining the Link Disk to its corresponding Alignment Ring. Right column are the recorded data at the Z− side.*

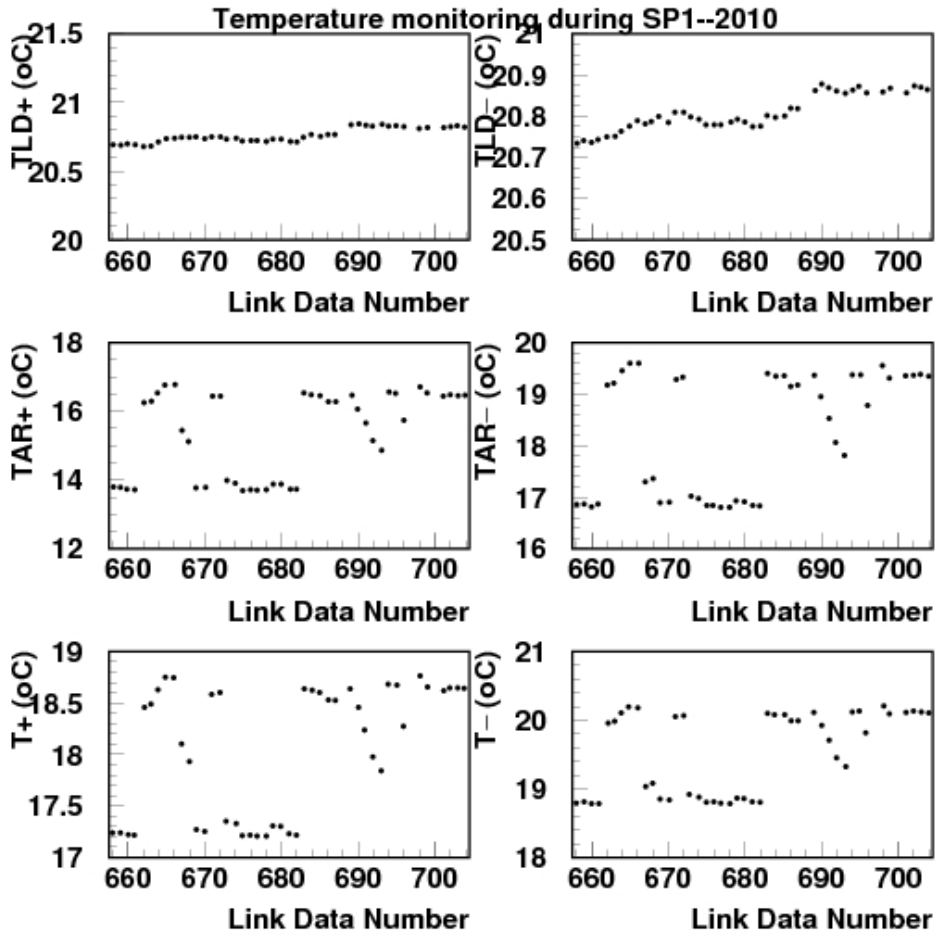

Fig 19: *Monitoring of the temperature during the SP1 in year 2010 as a function of the Link Data Number. Data are recorded twice per day. Most of the points represent two measurements superimposed. Left column corresponds to CMS Z+ side, the three plots represent the temperature measured near the Link Disk (6 PT100 sensors), the Alignment Ring (2 PT100 sensors) and the assumed temperature, T = (TLD + TAR)/2, in the air volume around the Long Profiles joining the Link Disk to its corresponding Alignment Ring. Right column are the recorded data at the Z− side.*

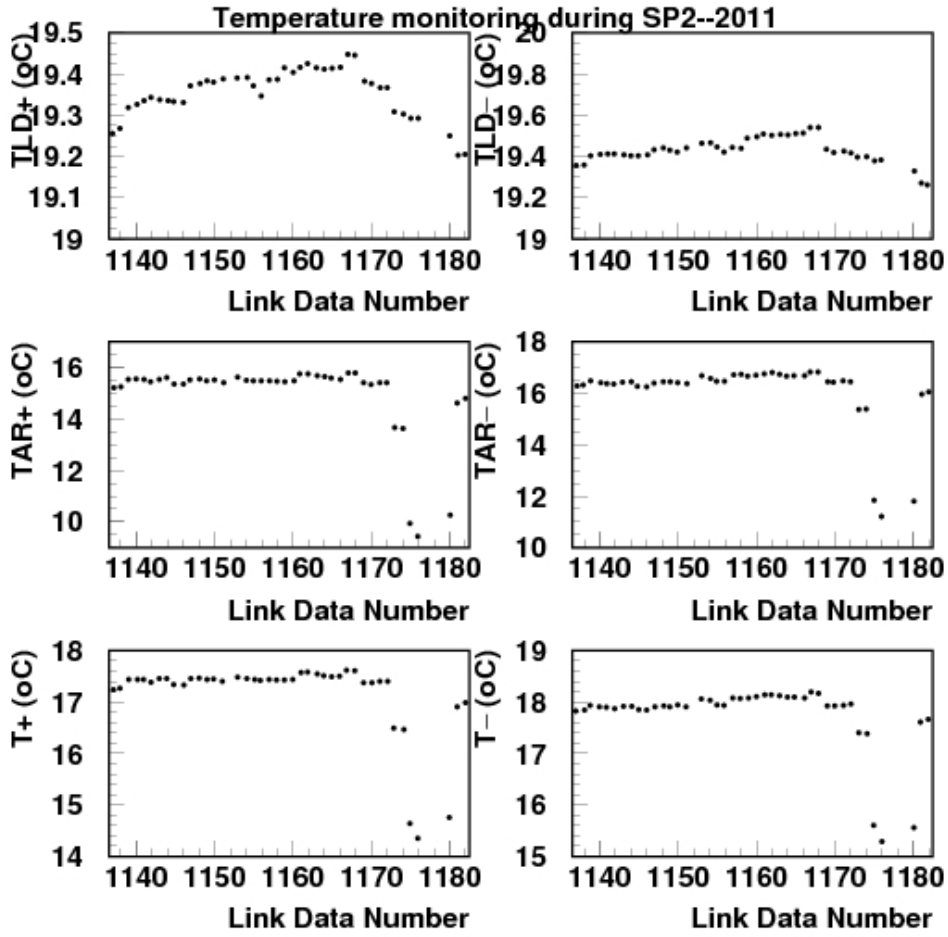

Fig 20: *Monitoring of the temperature during the SP2 in year 2011 as a function of the Link Data Number. Data are recorded twice per day. Most of the points represent two measurements superimposed. Left column corresponds to CMS Z+ side, the three plots represent the temperature measured near the Link Disk (6 PT100 sensors), the Alignment Ring (2 PT100 sensors) and the assumed temperature, T = (TLD+TAR)/2, in the air volume around the Long Profiles joining the Link Disk to its corresponding Alignment Ring. Right column are the, recorded data at the Z− side.*

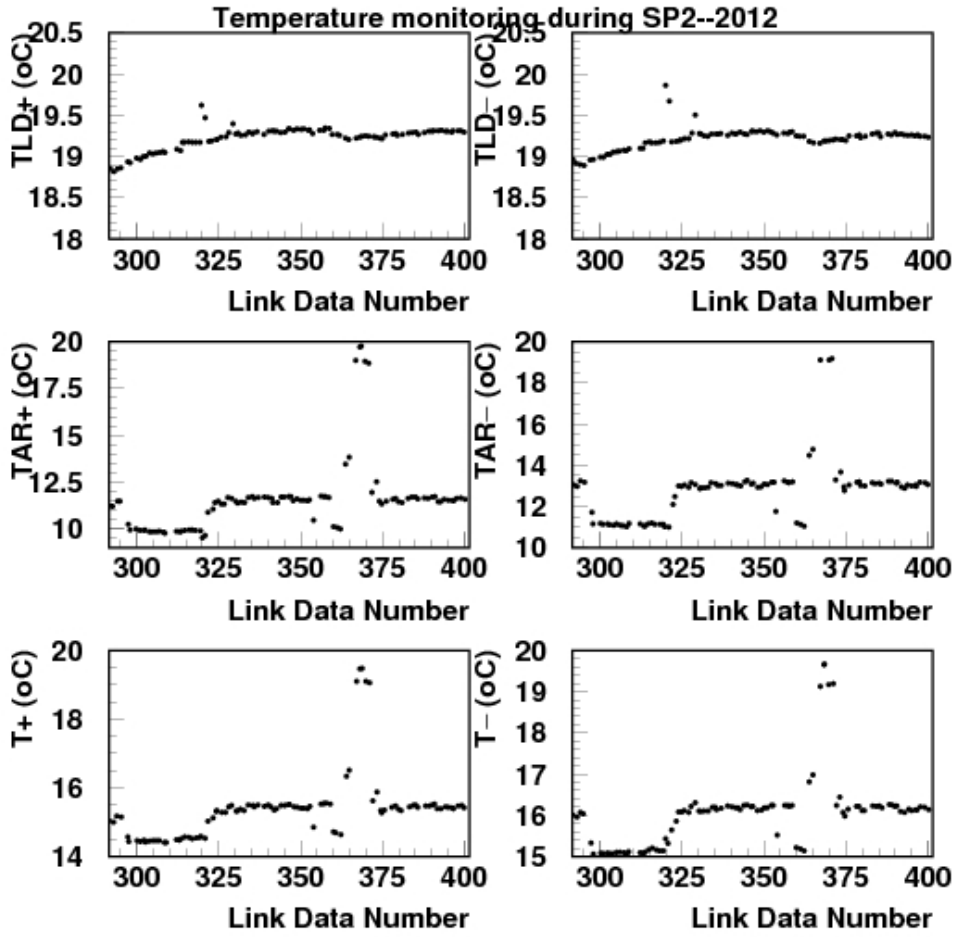

Fig 21: *Monitoring of the temperature during the SP2 in year 2012 as a function of the Link Data Number. Data are recorded twice per day. Most of the points represent two measurements superimposed. Left column corresponds to CMS Z+ side, the three plots represent the temperature measured near the Link Disk (6 PT100 sensors), the Alignment Ring (2 PT100 sensors) and the assumed temperature, T = (TLD + TAR)/2, in the air volume around the Long Profiles joining the Link Disk to its corresponding Alignment Ring. Right column are the, recorded data at the Z− side.*

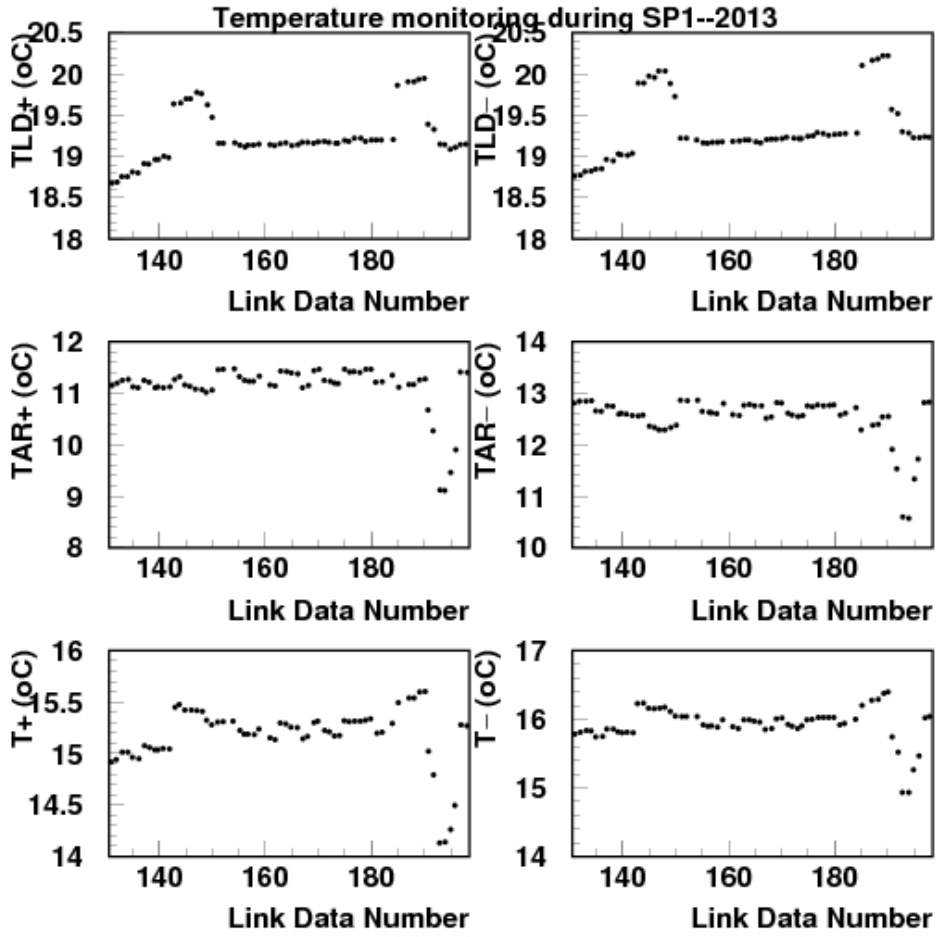

Fig 22: *Monitoring of the temperature during the SP1 in year 2013 as a function of the Link Data Number. Data are recorded twice per day. Most of the points represent two measurements superimposed. Left column corresponds to CMS Z+ side, the three plots represent the temperature measured near the Link Disk (6 PT100 sensors), the Alignment Ring (2 PT100 sensors) and the assumed temperature, T = (TLD + TAR)/2, in the air volume around the Long Profiles joining the Link Disk to its corresponding Alignment Ring. Right column are the, recorded data at the Z− side.*

As seen in the figures, the temperature in the LD and AR neighborhoods and therefore in the volume around the LPs, changes almost continuously, following strange patterns. While in the sets SP1-2008 (Fig. 17) and SP4-2009 (Fig. 18) the changes are just of a few tenths of ^{o}C, in the SP1-2010 (Fig. 19), SP2-2011 (Fig. 20) and SP2-2012 (Fig. 21) data sets one can appreciate changes of more than 1 ^{o}C, more than 2 ^{o}C in Fig. 20 for the set SP2-2011, and almost 4 ^{o}C in Fig. 21 for the set SP2-2012. The peculiar behavior of the monitored temperature along SP1-2013 (Fig. 22) shows a trend that may suggest the possible existence of some hot (at the LDs neighborhood) or cold (near the ARs) air flows.

At this point it is important to recall that a change of ±1 ^{o}C of the LPs represents a change of about ±86.6 μm in its length, twice the resolution of the short distances measurement potentiometers. Therefore, from the plots in Figs. 17 to 22 one can infer that the computed $\Delta Z(LD{-}AR) = Z(LD{-}AR)_{data\text{-}number} - Z(LD{-}AR)_{initial}$, in the corresponding data sets, would be affected by a systematic error of the order of $(T_i - T_{initial}) \times 86.6$ μm/^{o}C, where T_i is the recorded temperature when computing the Z(LD−AR) distance at the Link Data Number "i" and $T_{initial}$ the corresponding temperature for the first data in that particular SP. Therefore, any correlation between the measured ΔZ(LD−AR) and ΔT may explain the investigated "accordion" motion.

5.2 Looking for [ΔZ(LD−AR) – T] and [ΔZ(LD−AR) − ΔT] correlations.

A picture of ΔZ(LD−AR) as a function of the average temperature in the corresponding CMS Z side, at the time the measurement is done, is shown in Fig. 23. The gaps do not correspond to missing data but they are due to the changes in the temperature as the ones observed in Figs. 17 to 22.

The correlations between the monitored ΔZ(LD−AR) and the average temperature T of the involved LP, although clearly observed, are difficult to describe by a simple 24 μm per meter and degree centigrade parametrization of the LP length.

To illustrate this point Figs. 24 to 29 show, for the six data sets in Fig. 15, the following simultaneously monitored measurements: ΔZ(LD−AR) as a function of the Link Data Number (top plot), the temperature T in the air volume around of the Long Aluminium Profiles joining the Link Disks to their corresponding Alignment Rings in the given CMS Z side (TZ + or −) as a function of the Link Data Number (middle plot) and the ΔZ(LD−AR) of the top plot as a function of the reconstructed $\Delta T = (T_{data\text{-}number} - T_{initial})$ (bottom plot). The straight line over the data points corresponds to a linear fit to the data. The initial Z(LD−AR) and T values correspond to those of the first data taken, at the indicated (Φ, Z side) position, 24 hours after B_{max} is reached. The fitted function is of the type ΔZ (μm) = Constant (μm^{o}C^{-1}) × ΔT (^{o}C) + Offset (μm).

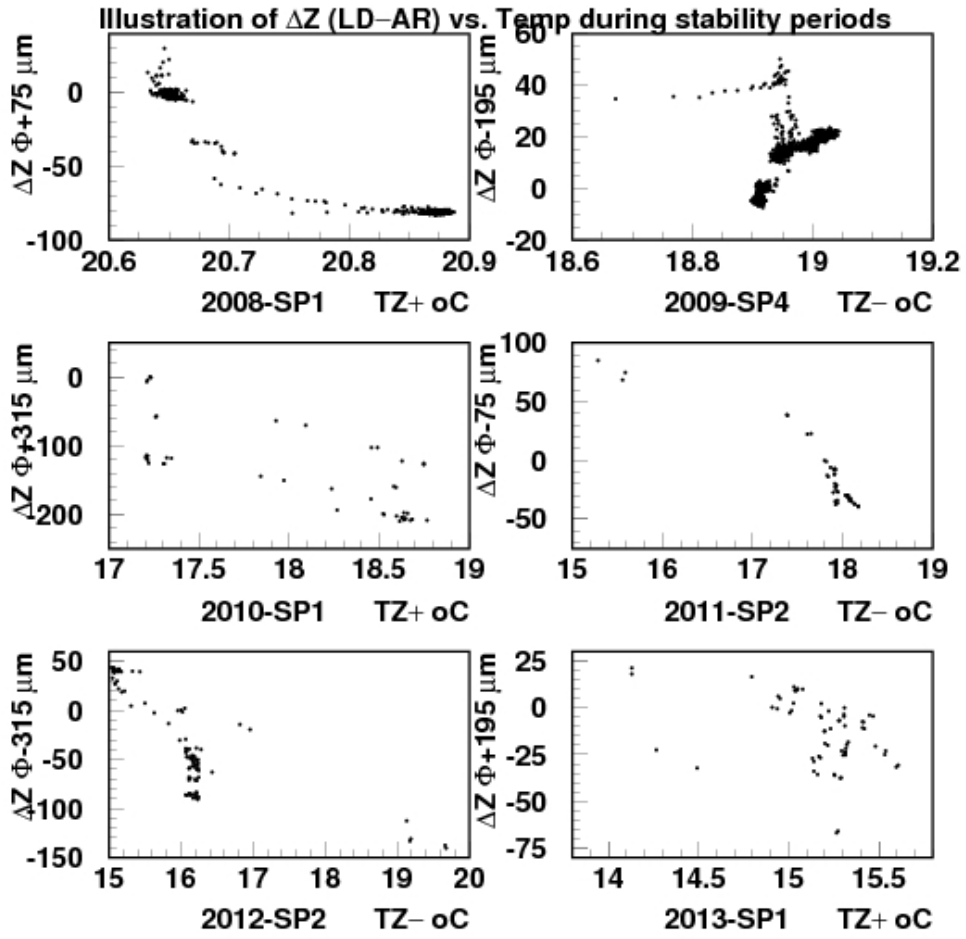

Fig 23: *ΔZ(LD-AR) distance measurements, in microns, for the indicated Φ quadrant (sign refers to + or – Z CMS side) versus the average temperature T, in ^{o}C, for the indicated CMS Z side (sign refers to the side), during the indicated Stability Period for the mentioned year. Although the correlations exist, their parametrization do not appear to be simple and unique.*

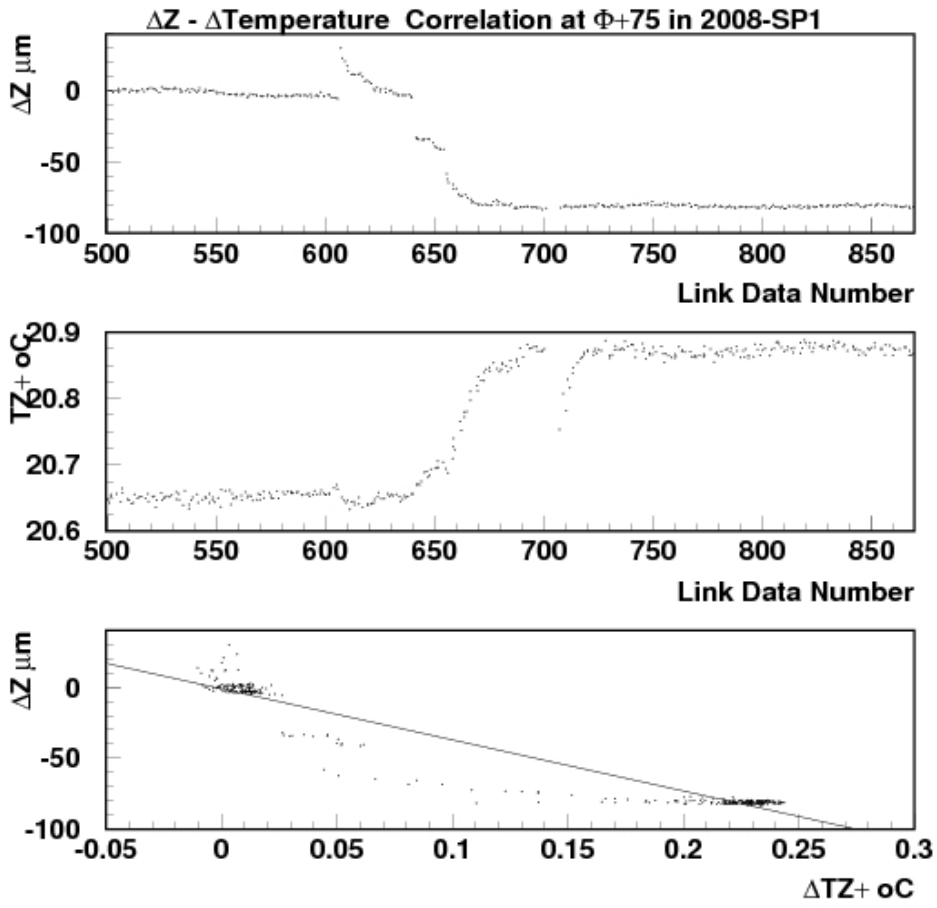

Fig 24: *Correlation of the measured ΔZ(LD-AR) with the changes in the temperature in the air volume around the Longitudinal Profiles. In the case of this example the relation between the two measured quantities, with respect to those of the first data taking during the SP1 in the year 2008 at Φ = +75, is ΔZ (μm) = (-360.7±20.0) (μm/°C) x ΔT (°C), with χ^2/NDF = 20/359. ΔT = T_{data} (°C) – 20.64 (°C). Data were recorded every five minutes.*

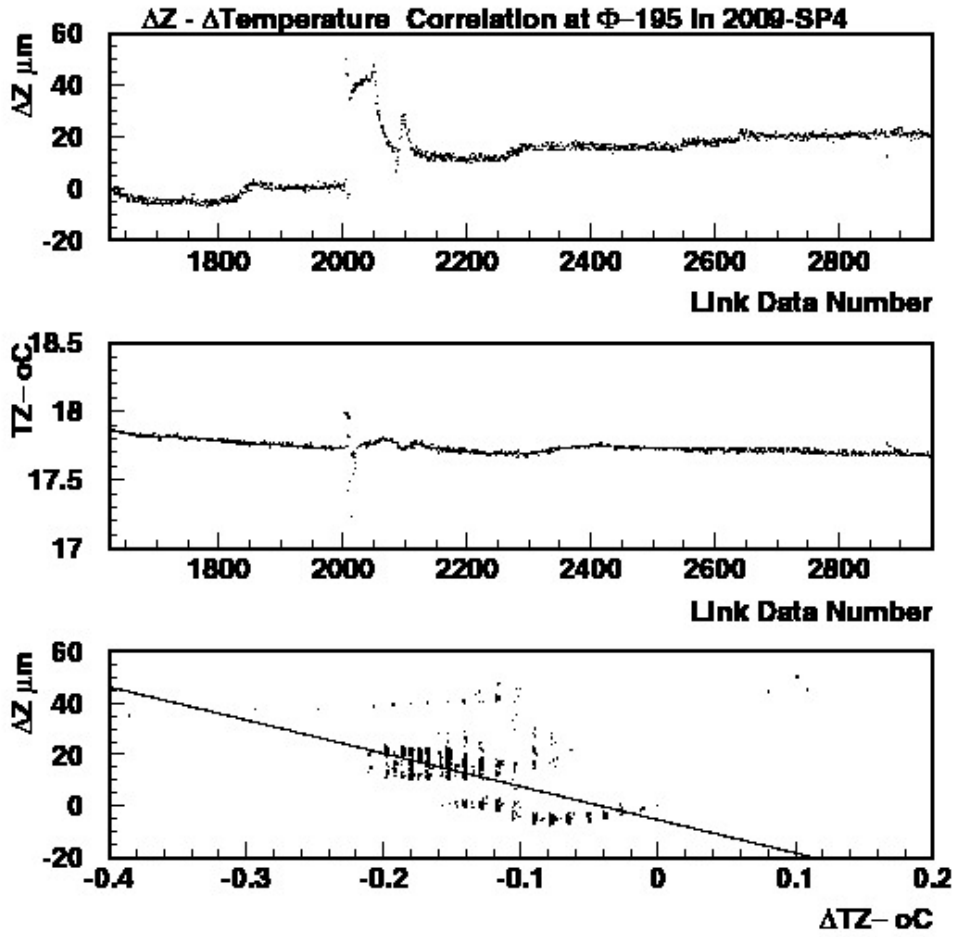

Fig 25: *Correlation of the measured ΔZ(LD-AR) with the changes in the temperature in the air volume around the Longitudinal Profiles. In the case of this example the relation between the two measured quantities, with respect to those of the first data taking during the SP4 in the year 2009 at Φ = −195, is ΔZ (μm) = (−129.2±23.3) (μm/°C) x ΔT (°C), with χ^2/NDF = 68/1309. ΔT = T_{data} (°C) – 17.88 (°C). Data were recorded every five minutes.*

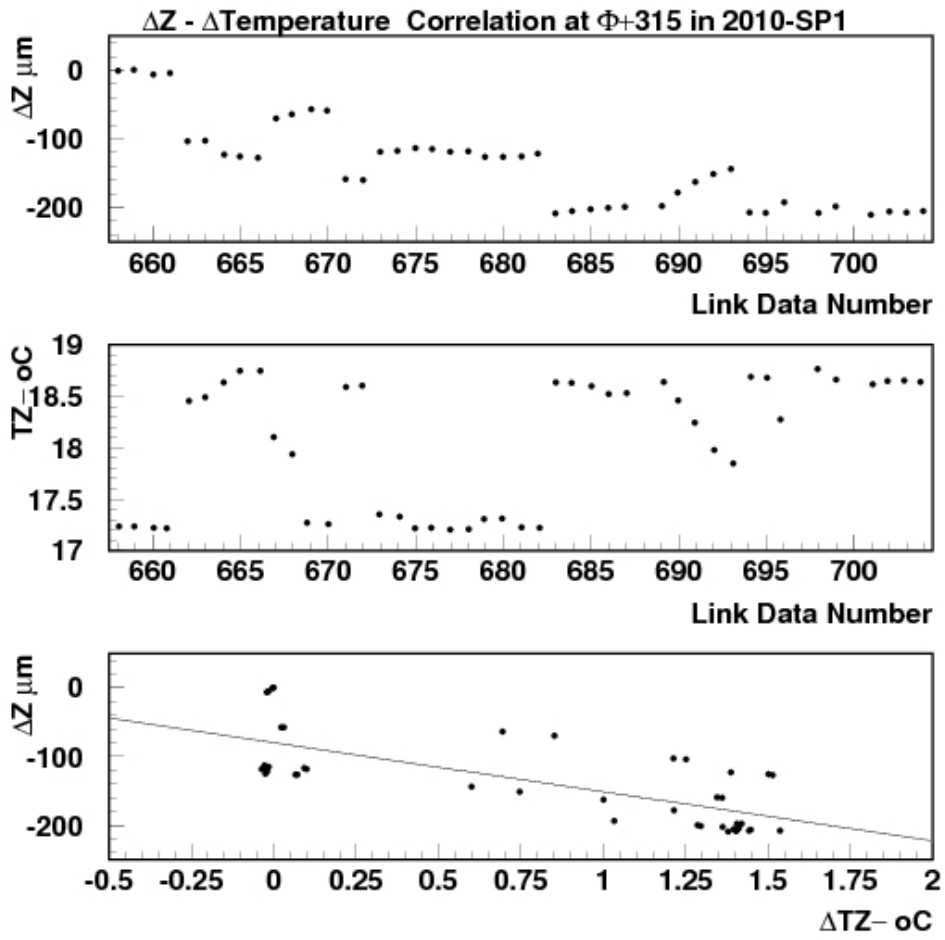

Fig 26: *Correlation of the measured ΔZ(LD-AR) with the changes in the temperature in the air volume around the Longitudinal Profiles. In the case of this example the relation between the two measured quantities, with respect to those of the first data taking during the SP1 in the year 2010 at Φ = +315, is ΔZ (μm) = (-71.6±9.5) (μm/°C) x ΔT (°C), with χ^2/NDF = 50/42. ΔT = T_{data} (°C) – 17.24 (°C).*

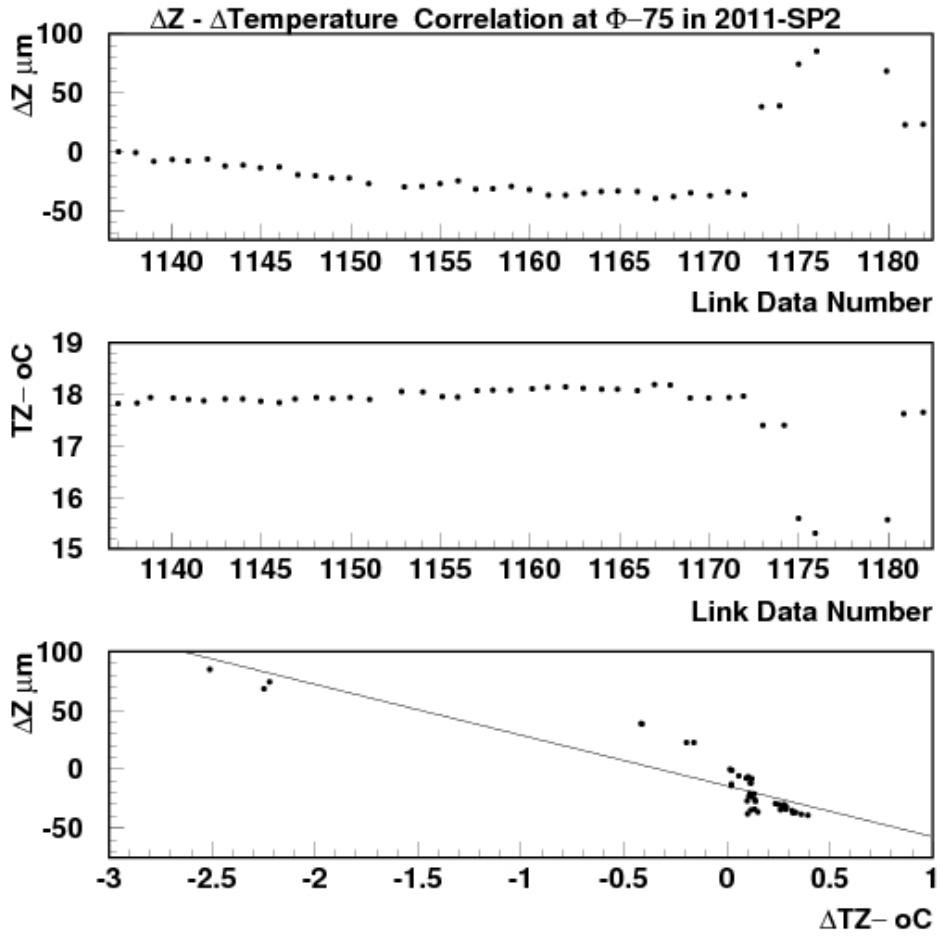

Fig 27: *Correlation of the measured ΔZ(LD-AR) with the changes in the temperature in the air volume around the Longitudinal Profiles. In the case of this example the relation between the two measured quantities, with respect to those of the first data taking during the SP2 in the year 2011 at Φ = –75, is ΔZ (μm) = (-43.2±9.4) (μm/°C) x ΔT (°C), with χ^2/NDF = 5/40. ΔT = T_{data} (°C) – 17.80 (°C).*

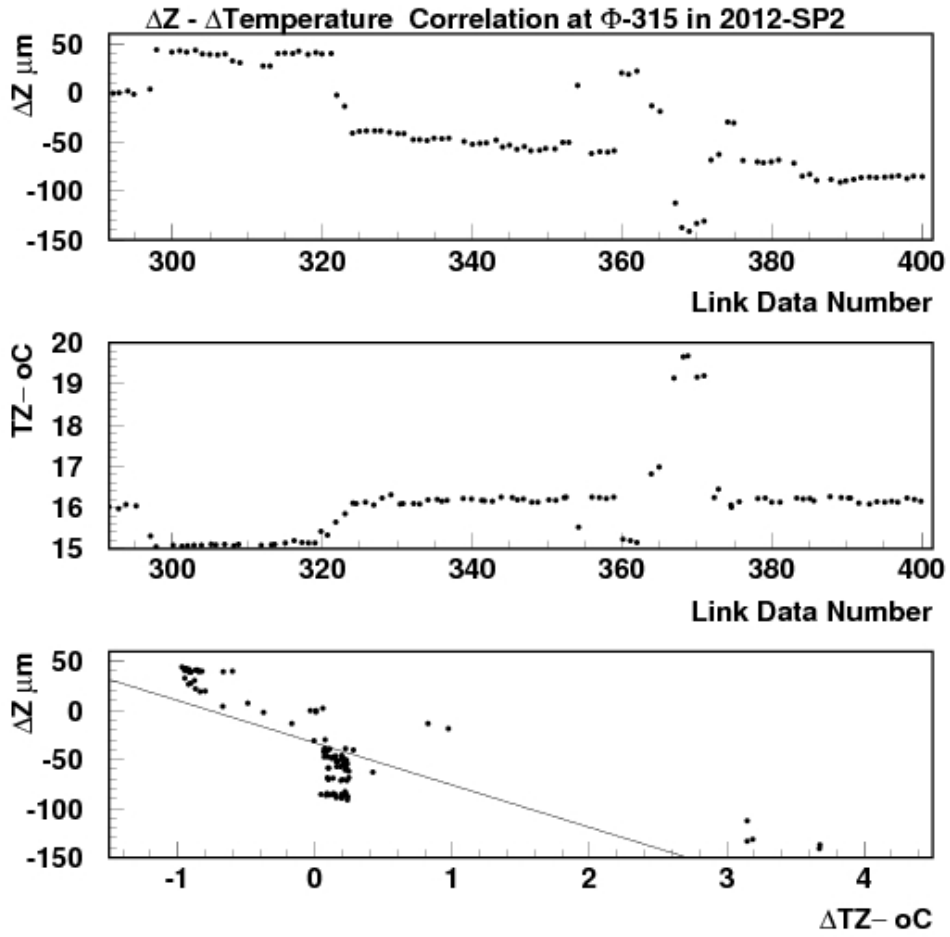

Fig 28: *Correlation of the measured ΔZ(LD-AR) with the changes in the temperature in the air volume around the Longitudinal Profiles. In the case of this example the relation between the two measured quantities, with respect to those of the first data taking during the SP2 in the year 2012 at Φ = –315, is ΔZ (μm) = (-43.1±4.5) (μm/°C) x ΔT (°C), with χ^2/NDF = 59/96. ΔT = T_{data} (°C) – 16.00 (°C).*

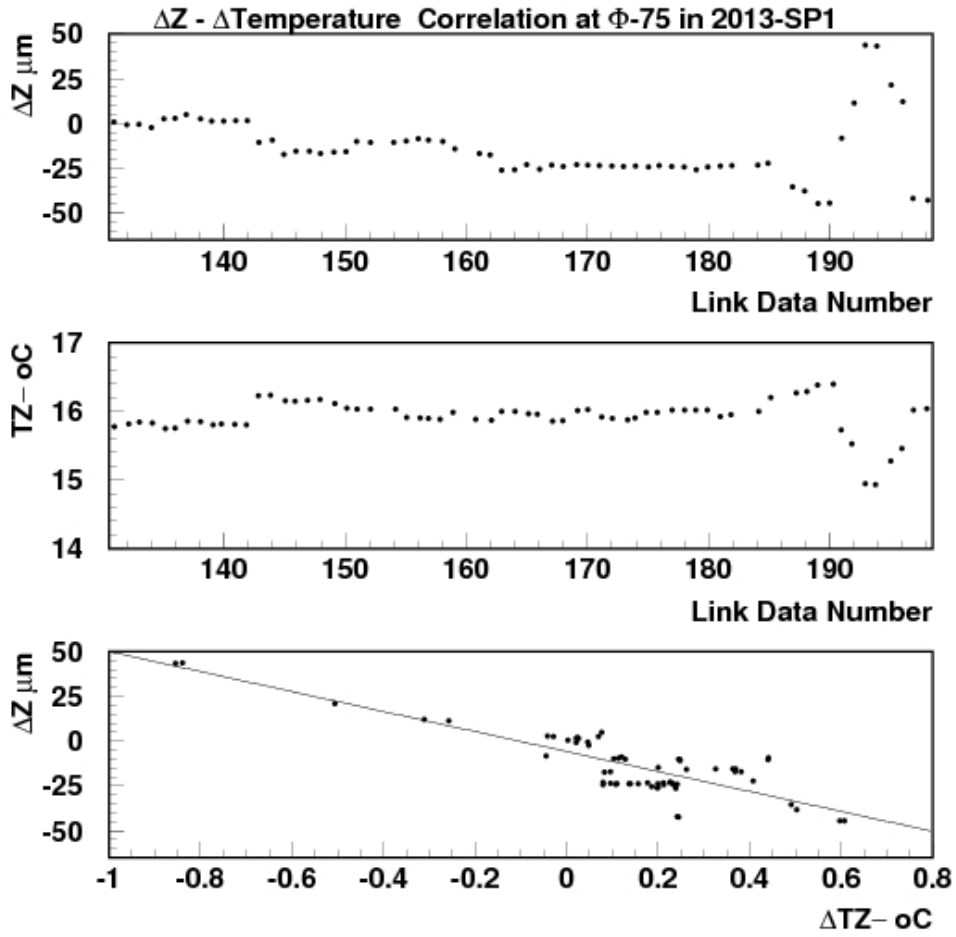

Fig 29: *Correlation of the measured ΔZ(LD-AR) with the changes in the temperature in the air volume around the Longitudinal Profiles. In the case of this example the relation between the two measured quantities, with respect to those of the first data taking during the SP1 in the year 2013 at Φ = –75, is ΔZ (μm) = (-55.8±19.3) (μm/°C) x ΔT (°C), with χ^2/NDF = 4/62. ΔT = T_{data} (°C) – 15.78 (°C).*

The ΔZ−ΔT correlation is quite clear: when the temperature increases with respect to the first value in the SP, the length of the affected aluminium profile (LP) increases, the potentiometers get compressed, and therefore the LD–AR relative distance appears to

decrease as if the LD approached the corresponding AR. This is the origin of the detected accordion motion: the core of CMS does not move during the Stability Periods, Link Disks and Alignment Rings do not move with respect to each other. The Longitudinal Profiles stretch or shrink according to the sign and the size of $\Delta T = (T_i - T_{initial})$ when recording data number "i".

For the six sets of data points used as illustration in this Section, the results of the fits to the data are given in the captions of Figs. 24 to 29. The offsets are omitted.

To increase the statistics, and for the same sets of OY−SP data, we have investigated the behaviour of the sextant $\Phi = 195^o$ at the +Z CMS side. Results are shown in Figs. 30 to 35. In each of these figures the plots of ΔZ (relative LD to AR distance) and T (at the appropriate CMS Z side) vs. the Link Data Number, as well as the ΔZ vs. the ΔT (with the linear fit superimposed to the data points), are shown. Again the fitted constant and the χ^2/NDF are given in the corresponding figure captions.

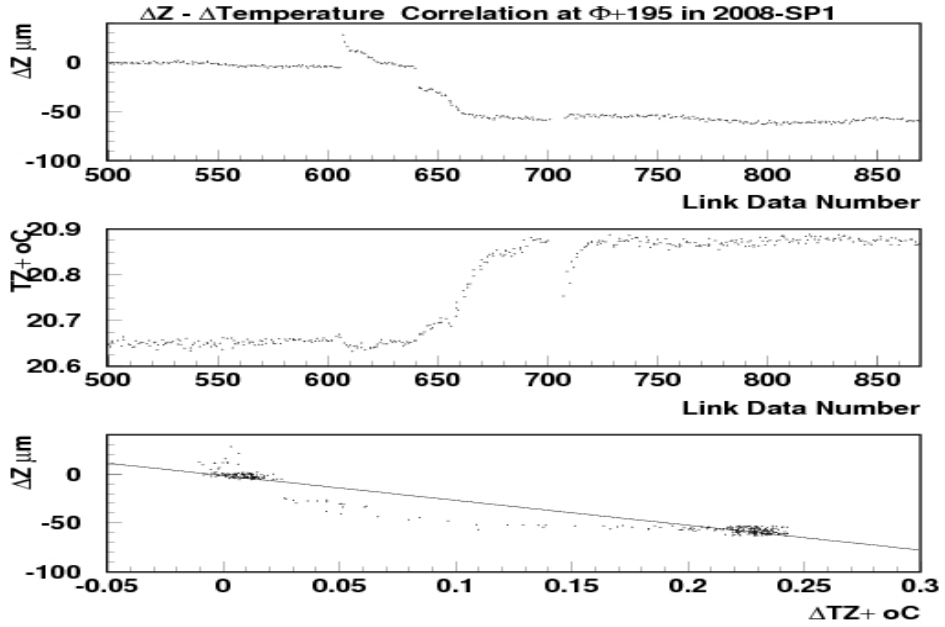

Fig 30: *Correlation of the measured ΔZ(LD-AR) with the changes in the temperature in the air volume around the Longitudinal Profiles. In the case of this example the relation between the two measured quantities, with respect to those of the first data taking during the SP1 in the year 2008 at Φ = +195, is ΔZ (μm) = (-253.7±20.0) (μm/°C) x ΔT (°C), with χ^2/NDF = 11/359. ΔT = T_{data} (°C) – 20.64 (°C). Data were recorded every five minutes. Results are almost identical to those in Fig. 25 as expected.*

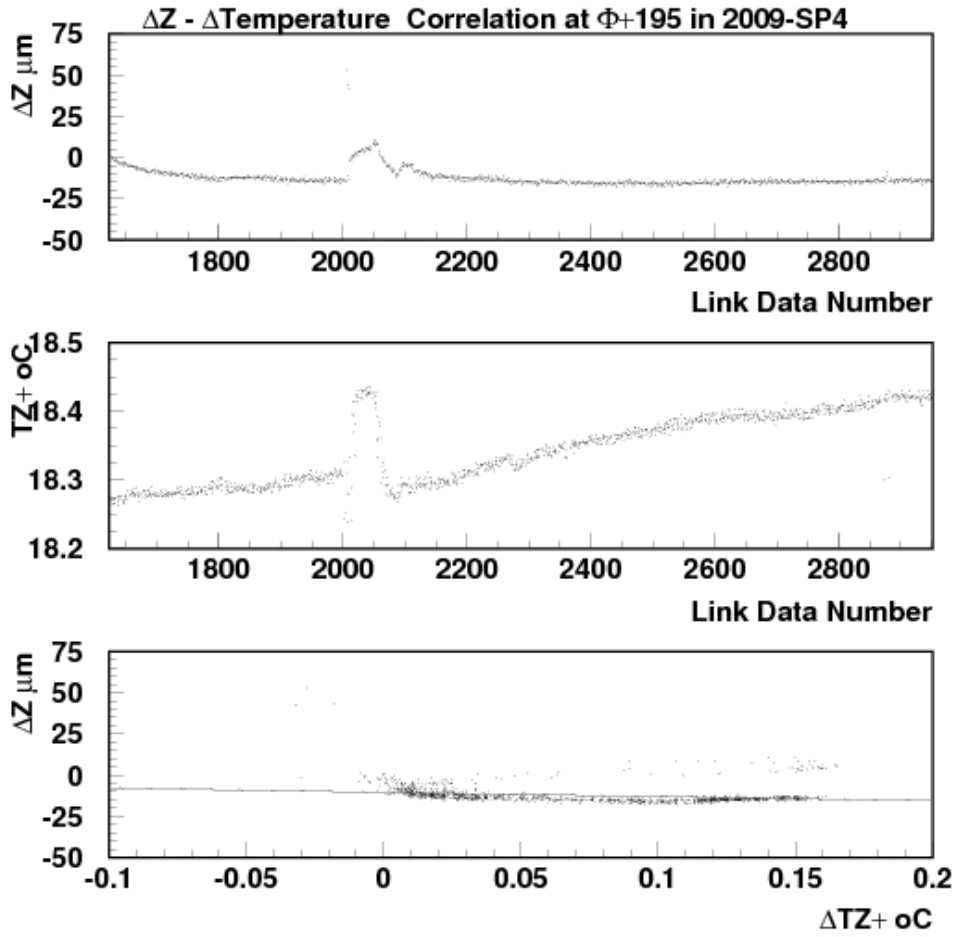

Fig 31: *Correlation of the measured ΔZ(LD-AR) with the changes in the temperature in the air volume around the Longitudinal Profiles. In the case of this example the relation between the two measured quantities, with respect to those of the first data taking during the SP4 in the year 2009 at Φ = +195, is ΔZ (μm) = (-25.6±21.7) (μm/°C) x ΔT (°C), with χ^2/NDF = 23/1309. ΔT = T_{data} (°C) – 18.27 (°C). Data were recorded every five minutes.*

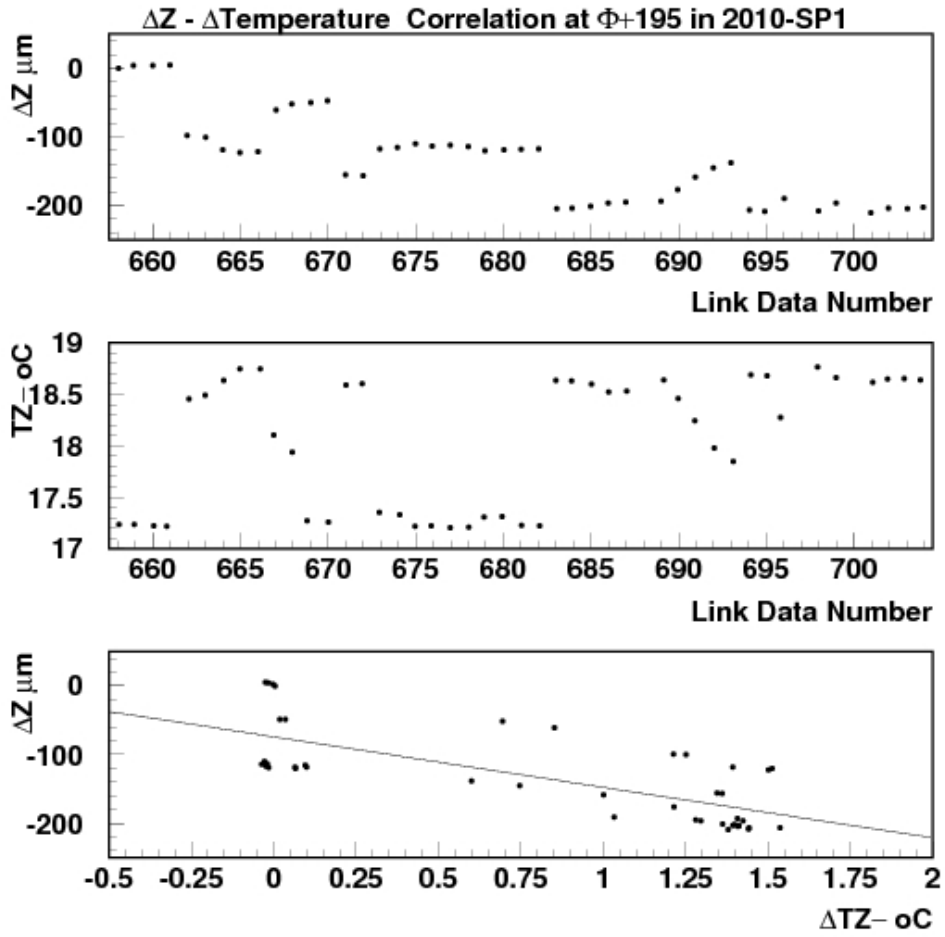

Fig 32: *Correlation of the measured ΔZ(LD-AR) with the changes in the temperature in the air volume around the Longitudinal Profiles. In the case of this example the relation between the two measured quantities, with respect to those of the first data taking during the SP1 in the year 2010 at Φ = +195, is ΔZ (μm) = (-73.7±2.4) (μm/°C) x ΔT (°C), with χ^2/NDF = 844/42. ΔT = T_{data} (°C) – 17.24 (°C). Results are almost identical to those in Fig. 26 as expected.*

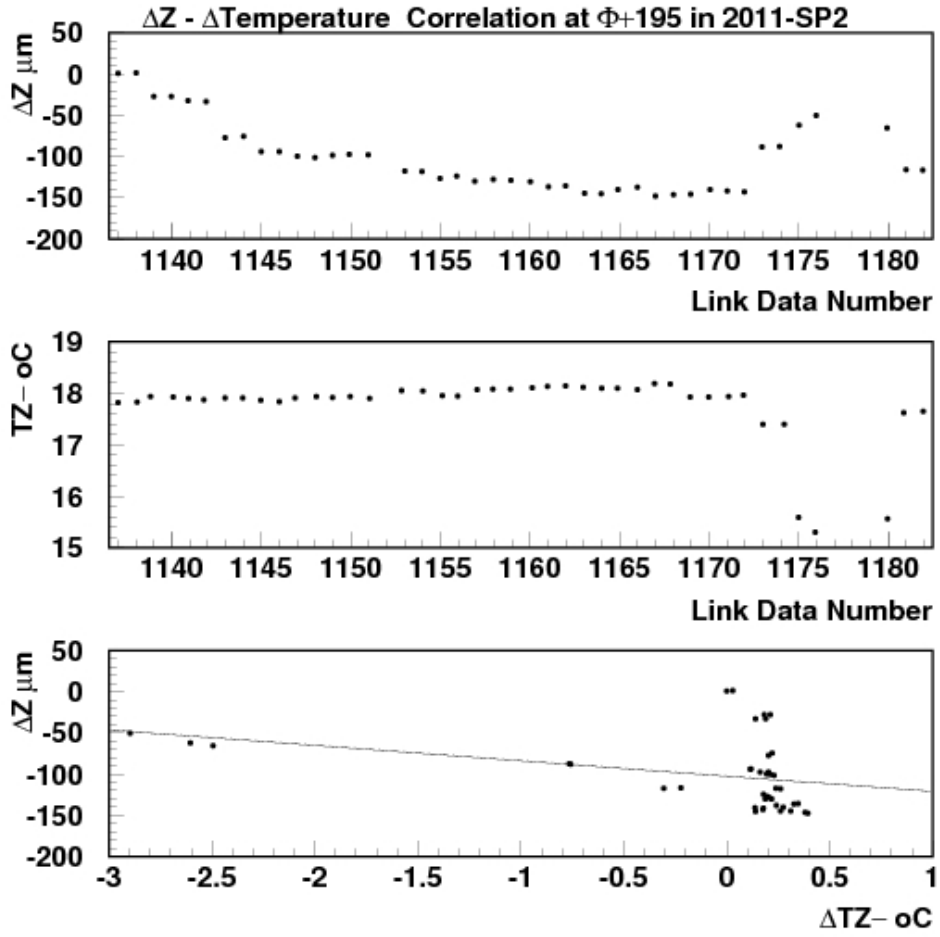

Fig 33: *Correlation of the measured ΔZ(LD-AR) with the changes in the temperature in the air volume around the Longitudinal Profiles. In the case of this example the relation between the two measured quantities, with respect to those of the first data taking during the SP2 in the year 2012 at Φ = +195, is ΔZ (μm) = (-18.7±8.1) (μm/°C) x ΔT (°C), with χ^2/NDF = 40/40. ΔT = T_{data} (°C) – 17.23 (°C).*

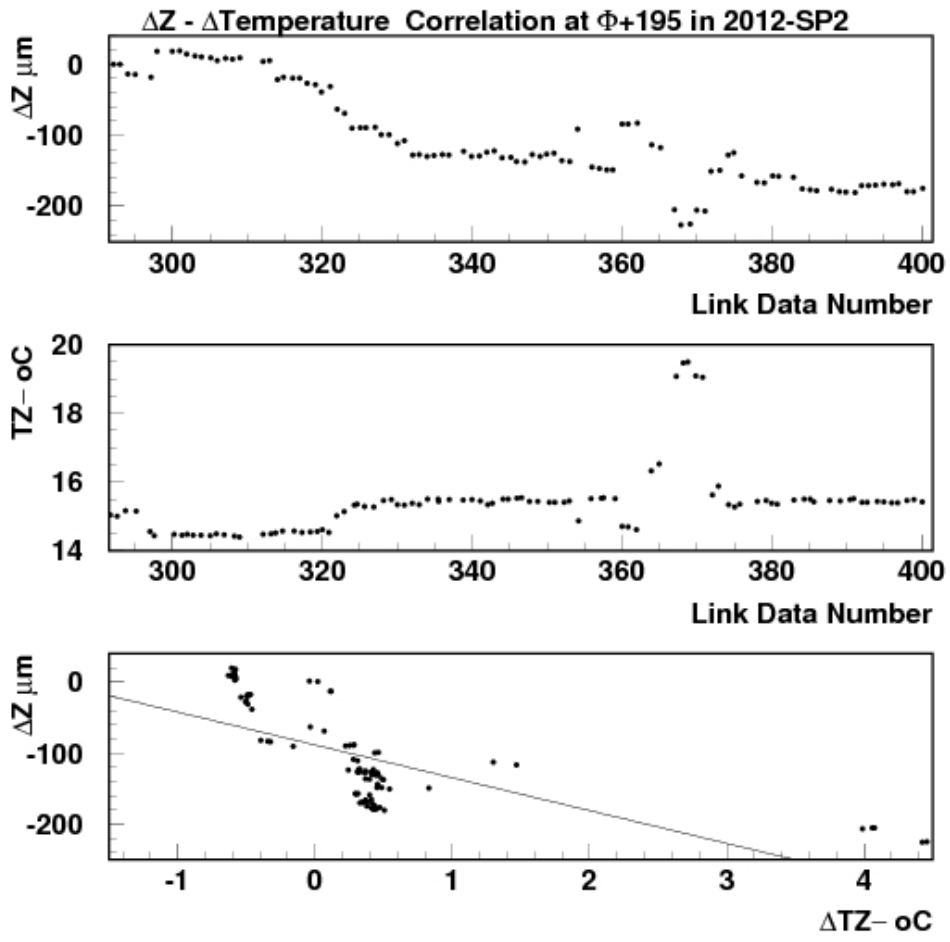

Fig 34: *Correlation of the measured ΔZ(LD-AR) with the changes in the temperature in the air volume around the Longitudinal Profiles. In the case of this example the relation between the two measured quantities, with respect to those of the first data taking during the SP2 in the year 2012 at Φ = +195, is ΔZ (μm) = (-46.3±4.1) (μm/°C) x ΔT (°C), with χ^2/NDF = 157/96. ΔT = T_{data} (°C) – 15.03 (°C).*

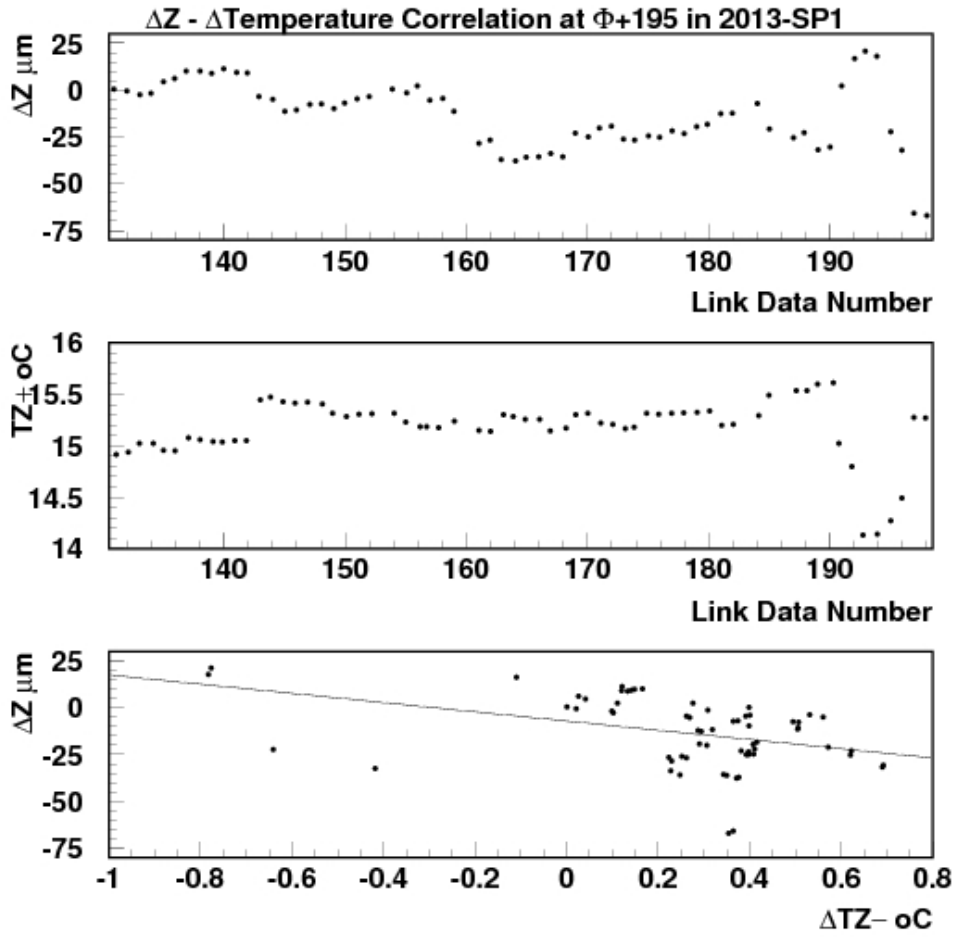

Fig 35: *Correlation of the measured ΔZ(LD-AR) with the changes in the temperature in the air volume around the Longitudinal Profiles. In the case of this example the relation between the two measured quantities, with respect to those of the first data taking during the SP1 in the year 2013 at Φ = +195, is ΔZ (μm) = (24.6±17.1) (μm/°C) x ΔT (°C), with χ^2/NDF = 11/62. ΔT = T_{data} (°C) – 14.91 (°C).*

The comparisons of the fitted constants for the 12 data sets with the expected "theoretical" value of 86.6 μm/°C are given in Table 21.

Year–SP#	(Zside) Φ (arc. deg.)	C_{fitted} (μm/°C)	χ^2/NDF	$T_{initial}$ (°C)
2008–SP1	+ 75	–360.7 ± 20.0	20/359	20.64
2008–SP1	+ 195	–253.7 ± 20.0	11/359	20.64
2009–SP4	– 195	–129.2 ± 23.3	68/1309	17.88
2009–SP4	+ 195	–25.6 ± 21.7	23/1309	18.27
2010–SP1	+ 315	–71.6 ± 9.5	50/42	17.24
2010–SP1	+ 195	–73.7 ± 9.5	53/42	17.24
2011–SP2	– 75	–43.2 ± 9.4	5/40	17.80
2011–SP2	+ 195	–18.7 ± 8.1	40/40	17.23
2012–SP2	– 315	–43.1 ± 4.5	59/96	16.00
2012–SP2	+ 195	–46.3 ± 4.1	157/96	15.03
2013–SP1	– 75	–55.8 ± 19.3	4/62	15.78
2013–SP1	+ 195	–24.6 ± 17.1	11/62	14.91

Table 21: *For the years and Stability Periods used in the text as examples and appearing in Column 1, and for the Zside/Φangle given in Column 2, results of the fitted C constants (Column 3) in the function ΔZ (μm) = C (μm/°C) × ΔT (°C) + O (μm), with ΔT = (T_i – $T_{initial}$), to be compared with the theoretical value $C_{expected}$ = 86.6 (μm/°C). Column 4 gives the χ^2/NDF of the corresponding fits. The input $T_{initial}$ (°C) value is given in Column 5. The offset (O) fitted value is considered irrelevant for the discussion.*

The value of $T_{initial}$, main input for the fit, is also given in the Table. The fact that, in most of the cases, the χ^2/NDF value results much smaller than 1, may suggest that the assigned error in the relative ΔZ distance (40 μm for every data point) in the χ^2 function is somehow overestimated and that the Sakae potentiometer may be more precise than assumed.

Although the fits are quite bad in many cases (the effect of the temperature changes in the assembly LD-LP-potentiometer-AR is probably too complex to be represented by a single constant) they clearly evidence the existence of ΔZ–ΔT correlations that are enough to explain the apparent CMS instability during the mechanical equilibrium periods. In fact we can conclude that CMS was fully stable during the data taking all along the first six years operation.

6. Results from the monitoring of the variables assumed to be mechanically stable: some examples

Throughout this document it was assumed that, excluding the LD to AR relative distance largely discussed in the previous sections, after the first 24 h at B_{max}, CMS was *absolutely* stable, i.e. all possible motions, translations and tilts, stayed within the resolution measurement, ± 40 μm for displacements and ± 40 μrad for rotations.

To verify the above statement a check is done on the recorded measurements corresponding to the following variables (see Fig. 4): i) the relative axial distance between the Transfer Plates (TPs) and their nearest ME/1/1 Endcap Muon Chamber, ΔZ(TP−ME11), ii) the relative radial distance between the external MABs and their nearest ME/1/2 Endcap Muon Chamber, ΔR(MAB−ME12), iii) the relative radial distance between the TPs and their nearest ME/1/2, ΔR(TP−ME12) and iv) the angular rotations of the Barrel Muon Chambers (see also Fig. 5). Each observable is measured at the six Φ sectors (15, 75, 135, 195, 255 and 315 arc. deg. respectively) at both CMS Z sides.

The present study uses, as in previous sections, the six sets of Operation Year/Stability Period (OY−SP) data: 2008−SP1, 2009−SP4, 2010−SP1, 2011−SP2, 2012−SP2 and 2013−SP1 (see Tables 7 – 12).

6.1 The relative axial distance between the Transfer Plates and their nearest ME/1/1 Endcap Muon Chamber, ΔZ(TP−ME11)

The Z(TP−ME11) distance is measured by a contact Sakae potentiometer installed in the Transfer Plate touching a target located on the top side of the ME/1/1 Endcap Muon Chamber as sketched in Fig. 4.

The observed axial motion between the TP and the ME11 when the field magnet goes from 0 to 3.8 T (years 2009 to 2013) indicates that TP moves apart (see Fig. 2) from ME11 an average value of $\langle Z \rangle = 1262.0 \pm 305.8$ μm at the CMS Z+ side, while for Z− the averaged displacement was $\langle Z \rangle = 1540.5 \pm 244.9$ μm. The quoted errors are only statistical (the RMS of the various measurements) and show how different can be the displacement from sector to sector in Φ.

The relative ΔZ(TP−ME11) distance is calculated, as in previous cases, by $\Delta Z(TP-ME11) = Z(TP-ME11)_{data\text{-}number} - Z(TP-ME11)_{initial}$ where the $Z(TP-ME11)_{initial}$ value corresponds to the first data taken, at each of the twelve Φ positions, 24 hours after B_{max} is reached in each of the OY−SP considered.

The evolution of the ΔZ(TP−ME11) relative distance as a function of the Link Data Number is illustrated on Fig. 36, for different Φ sectors.

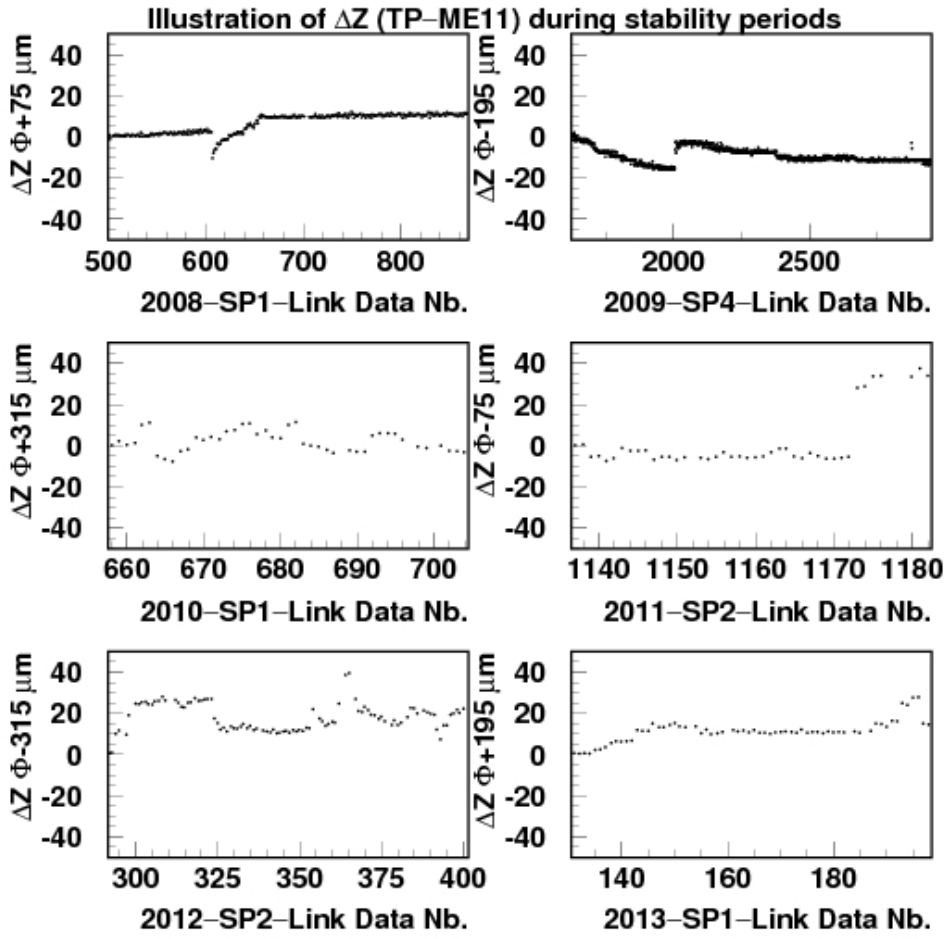

Fig 36: *Evolution of the ΔZ(TP–ME11) relative distance (vertical axis, in μm) as a function of the Link Data Number proper to the considered OP–SP data set, for different Φ sectors.*

Although the Z measurement is given just by the rod motion of the potentiometer (see Fig. 4), the small changes in the relative TP–ME/1/1 axial distance seems to be also correlated with the temperature at the central CMS volume as can be appreciate when looking at Fig. 16 that shows the evolution of the mean temperature during the same

OY−SP in the same CMS Z−sides. This fact gives to the CMS temperature changes an important role for mechanical motions measurements.

Nevertheless, motions stay inside the 40 μm short distance measurements resolution and therefore CMS is pretty stable 24 h after B_{max} is reached. This remains true for all sectors in the six OY−SP data taking periods as shown in Table 22, where the extreme value of the corresponding ΔZ distribution is given for the six sectors in the six OY−SP checked. In Table 22 the mention OO means that the sensor was *out of order* during the corresponding data period.

OY/SP	±Φ/ΔZ	±Φ/ΔZ	±Φ/ΔZ	±Φ/ΔZ	±Φ/ΔZ	±Φ/ΔZ
2008/SP1	+15/10.0	+75/12.4	+135/20.0	+195/OO	+255/OO	+315/6.8
	−15/10.0	−75/-15.1	−135/14.1	−195/-10.7	−255/10.0	−315/12.7
2009/SP4	+15/-12.3	+75/-15.1	+135/-15.0	+195/-15.0	+255/-39.7	+315/-11.4
	−15/-17.1	−75/-23.2	−135/-30.5	−195/-16.2	−255/-12.0	−315/-10.7
2010/SP1	+15/10.6	+75/18.0	+135/24.6	+195/16.1	+255/OO	+315/12.0
	−15/-16.1	−75/-30.2	−135/-23.6	−195/21.0	−255/16.7	−315/15.7
2011/SP2	+15/23.8	+75/27.8	+135/20.8	+195/18.7	+255/OO	+315/15.0
	−15/21.9	−75/37.9	−135/26.8	−195/15.0	−255/14.8	−315/25.1
2012/SP2	+15/27.0	+75/35.0	+135/35.2	+195/24.3	+255/OO	+315/26.5
	−15/37.7	−75/OO	−135/OO	−195/27.8	−255/35.8	−315/38.9
2013/SP1	+15/21.5	+75/38.3	+135/30.0	+195/6.5	+255/OO	+315/22.3
	−15/27.4	−75/31.6	−135/33.3	−195/31.6	−255/33.3	−315/23.3

Table 22: *For the years and Stability Periods used in the text as examples, indicated by OY/SP in Column 1, the extreme value of the ΔZ(TP−ME11) distribution is given, in μm, for the analyzed ±Φ sector. The sign in front of the Φ value indicates the CMS Z side. The angle Φ is given in arc. deg. A negative sign in the ΔZ value would correspond to a TP to ME/1/1 mechanical approach while a positive value would evidence that TP and ME/1/1 move apart. However, these apparent motions may also be a manifestation of small temperature changes in the area.*

A negative sign in the ΔZ value would correspond to a TP to ME/1/1 mechanical approach while a positive value would evidence that TP and ME/1/1 move apart. However, the correspondence between the LD to AR motions and the simultaneous

temperature changes during the data taking may suggest that also in the case of the TPs and their nearest ME/1/1 chamber apparent motions may be a manifestation of small temperature changes in the area.

6.2 The relative radial distance between the Transfer Plates and their nearest ME/1/2 Endcap Muon Chamber, ΔR(TP−ME12)

The radial distance between the TP and the bottom side of its nearest ME/1/2 chamber, R(TP−ME12), is also monitored using a contact potentiometer as sketched in Fig. 4.

The observed radial motion between the TP and the ME12 Chamber, when the field magnet goes from 0 to 3.8 T (years 2009 to 2013) indicates that TP moves apart (see Fig. 2) from ME12 an average value of $\langle R \rangle = 2764.4 \pm 236.5$ μm at the CMS Z+ side, while for Z− the averaged displacement was $\langle R \rangle = 2883.5 \pm 246.3$ μm. The quoted errors are only statistical (RMS of the different measurements) and evidence also for this radial displacement how different they can be from sector to sector in Φ.

The relative ΔR(TP−ME12) distance is calculated, as in previous cases, by $\Delta R(TP-ME11) = R\ (TP-ME11)_{data\text{-}number} - R(TP-ME11)_{initial}$ where the $R(TP-ME11)_{initial}$ value corresponds to the first data taken, at each of the twelve Φ positions, 24 hours after B_{max} is reached in each of the OY−SP considered.

How the ΔR(TP−ME12) value evolves as a function of the Link Data Number proper to the considered data set is illustrated in Fig. 37, for the same Φ sectors used to illustrate the ΔZ(TP−ME11) motion.

Comparing Fig. 37 with the previous Fig. 36 is easy to identify simultaneous motions that accompany the recalled temperature changes. Although the effect is again very small (stays within the measurement resolution of the potentiometers) it nevertheless remains visible.

Table 23 displays the extreme values of the ΔR(TP−ME12) distributions for the six Φ sectors in the six OY−SP checked. Here one should also recall that a negative sign in the ΔR value would correspond to a TP to ME/1/2 mechanical approach while a positive value would evidence that TP and ME/1/2 move apart. However, it is very plausible that the TPs and their nearest ME/1/2 chamber apparent radial motions may also be a consequence of small temperature changes in the area.

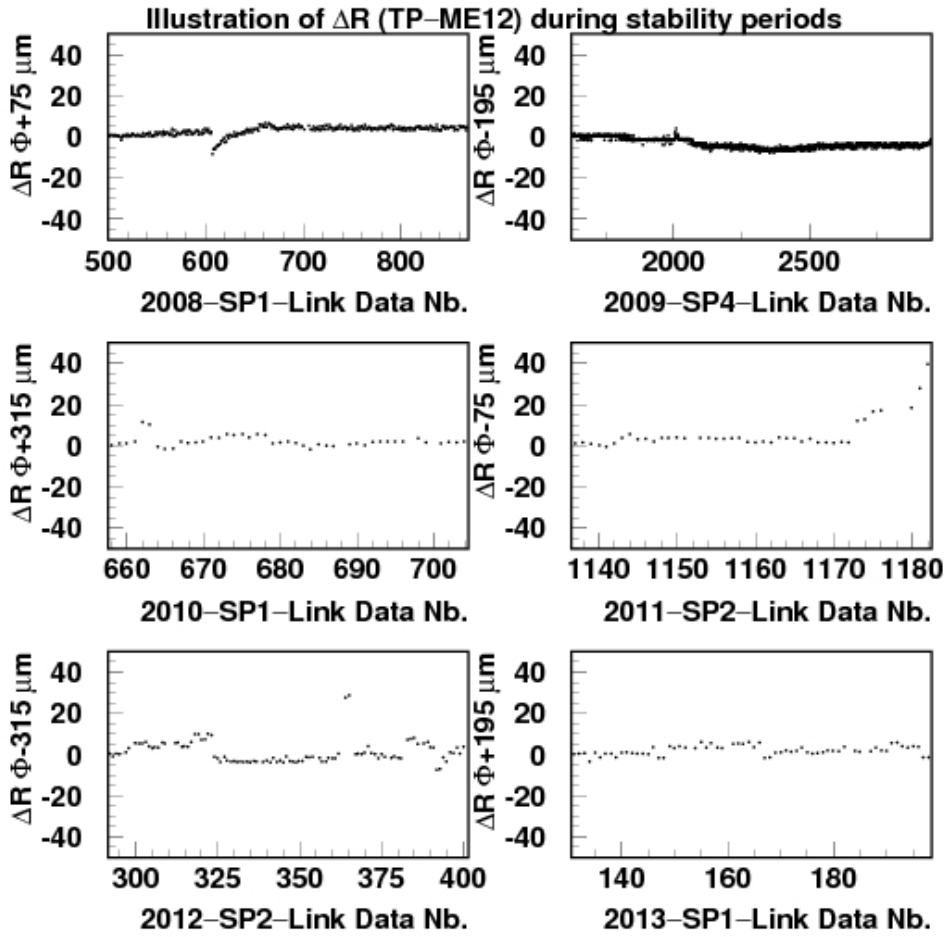

Fig. 37: *Evolution the ΔR(TP–ME12) value (vertical axis, in μm) as a function of the Link Data Number proper to the considered data set for the same Φ sectors used to illustrate the ΔZ(TP–ME11) motion on Fig. 36.*

OY/SP	±Φ/ΔR	±Φ/ΔR	±Φ/ΔR	±Φ/ΔR	±Φ/ΔR	±Φ/ΔR
2008/SP1	+15/-10.5	+75/-11.5	+135/-7.9	+195/OO	+255/-15.3	+315/-10.0
	−15/-9.7	−75/-10.0	−135/-7.8	−195/20.0	−255/-12.0	−315/-11.1
2009/SP4	+15/-4.6	+75/-9.1	+135/12.8	+195/-7.7	+255/-6.0	+315/6.4
	−15/8.8	−75/-14.3	−135/-10.1	−195/-8.0	−255/-25.3	−315/-6.6
2010/SP1	+15/20.8	+75/22.9	+135/-13.1	+195/11.9	+255/11.8	+315/11.6
	−15/23.8	−75/-11.0	−135/-14.2	−195/-5.8	−255/29.8	−315/16.1
2011/SP2	+15/34.7	+75/35.2	+135/33.5	+195/22.5	+255/29.6	+315/31.7
	−15/21.5	−75/39.8	−135/34.4	−195/33.5	−255/OO	−315/33.2
2012/SP2	+15/7.0	+75/7.6	+135/24.9	+195/11.6	+255/14.4	+315/7.9
	−15/14.7	−75/20.8	−135/18.4	−195/15.4	−255/27.8	−315/10.2
2013/SP1	+15/6.5	+75/25.5	+135/21.6	+195/5.5	+255/13.6	+315/6.3
	−15/17.6	−75/21.5	−135/24.0	−195/3.9	−255/25.5	−315/16.8

Table 23: *For the years and Stability Periods used in the text as examples, indicated by OY/SP in Column 1, the extreme value of the ΔR(TP–ME12) distribution is given, in μm, for the analyzed ±Φ sector. The sign in front of the Φ value indicates the CMS Z side. The angle Φ is given in arc. deg. A negative sign in the ΔR value would correspond to a TP to ME/1/2 mechanical approach while a positive value would evidence that TP and ME/1/2 move apart. However, these apparent motions may also be a manifestation of small temperature changes in the area.*

6.3 The relative radial distance between the External MABs and their nearest ME/1/2 Endcap Muon Chamber, ΔR(MAB–ME12)

The radial distance between the MAB and the outer side of the ME/1/2 chamber is monitored using a non-contact proximity sensor (Omron [12]) installed at the innermost part of each MAB structure. The sensor emitting/receiving head directs a laser light and receives the reflected light to/from a reflective target located on the outer region of the ME/1/2 chamber, as sketched in Fig. 4.

In this case, when the magnetic field increases from 0 to 3.8 T, the External MABs approach their corresponding ME/1/2 Chambers (see Fig. 2) in a very small amount, <R> = −274.5 ± 34.6 μm at the CMS Z+ side, while for Z− the measured averaged displacement was <R> = −262.8 ± 31.8 μm. The negative sign indicates that both

structures approach each other. There is no evidence of positive/negative asymmetry for this radial motion.

For the relative displacements, as in previous subsections, the used function was $\Delta R(MAB{-}ME12) = R\ (MAB{-}ME12)_{data\text{-}number} - R(MAB{-}ME12)_{initial}$ where the $R(MAB{-}ME12)_{initial}$ value corresponds to the first data taken, at each of the twelve Φ positions, 24 hours after B_{max} is reached in each of the OY−SP considered.

Fig. 38 illustrates, for some Φ sectors at positive and negative CMS Z sides during the considered OY−SP data taking periods, the recorded data as a function of the Link Data number. For this variable we have chosen symmetric Φ sectors with respect to the CMS center.

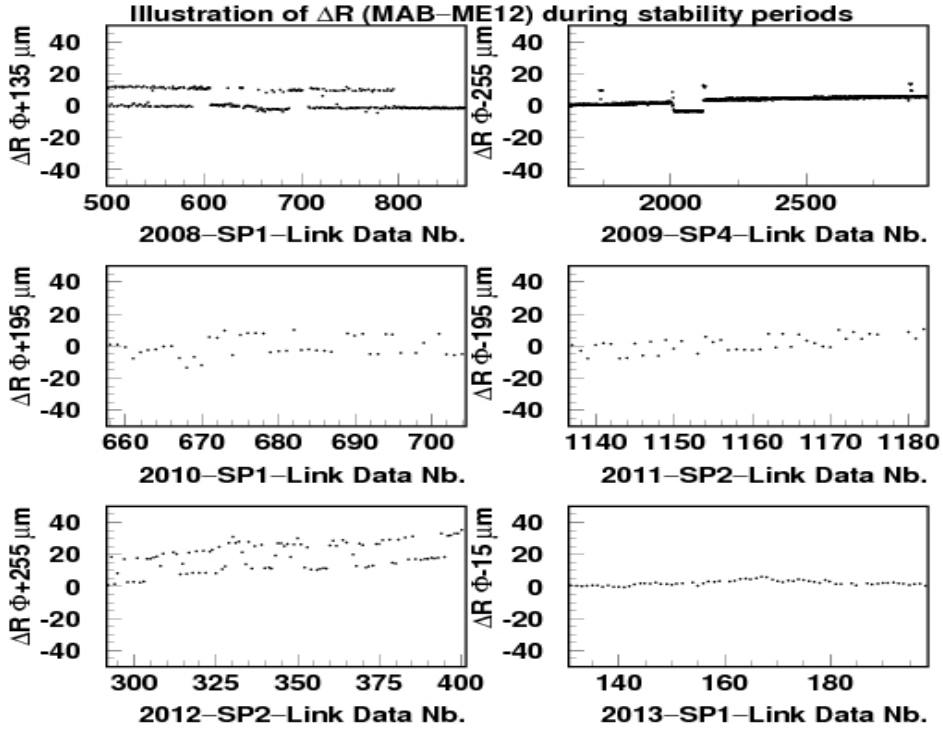

Fig. 38: *Relative ΔR(MAB-ME12) radial distance (vertical axis, in μm) as a function of the Link Data number for some Φ sectors at positive and negative CMS Z sides during the considered OY−SP data taking periods. For this illustration we have chosen sectors showing the greatest measured motions.*

Clearly, the non-contact measuring sensors are not influenced by the temperature (that, in fact, is not monitored at the level of the Barrel Muon Chambers), but, for the years 2010 to 2012, the MAB to ME12 relative distances increases, in a monotone way, with time (Link Data Number). In addition, a data-to-data 10 to 20 μm differences can be appreciated. The origins of both phenomena remain unclear. In any case, the plotted ΔR values in Fig. 38, and the corresponding quoted values on Table 24 all remain within the measurement resolution for the used sensors (±40 μm as well), but one data in the 2010−SP1 at sector $\Phi = -255^{o}$ that exhibits a value of 40.9 μm (see Fig. 39).

OY/SP	±Φ/ΔR	±Φ/ΔR	±Φ/ΔR	±Φ/ΔR	±Φ/ΔR	±Φ/ΔR
2008/SP1	+15/1.8	+75/OO	+135/11.8	+195/15.0	+255/13.7	+315/-5.1
	−15/OO	−75/OO	−135/20.0	−195/10.9	−255/20.0	−315/OO
2009/SP4	+15/-2.3	+75/OO	+135/13.2	+195/-13.2	+255/14.3	+315/2.1
	−15/OO	−75/OO	−135/OO	−195/-10.3	−255/15.1	−315/-4.7
2010/SP1	+15/7.1	+75/8.2	+135/-13.1	+195/-14.2	+255/-12.4	+315/4.9
	−15/10.0	−75/OO	−135/OO	−195/20.0	**−255/40.9**	−315/10.9
2011/SP2	+15/OO	+75/6.8	+135/-13.1	+195/-15.3	+255/-15.4	+315/6.8
	−15/10.1	−75/OO	−135/OO	−195/10.9	−255/37.4	−315/OO
2012/SP2	+15/OO	+75/20.5	+135/33.2	+195/33.2	+255/36.7	+315/OO
	−15/4.9	−75/OO	−135/OO	−195/24.9	−255/OO	−315/OO
2013/SP1	+15/OO	+75/15.9	+135/-8.5	+195/14.3	+255/15.3	+315/-4.6
	−15/5.4	−75/OO	−135/OO	−195/9.4	−255/OO	−315/OO

Table 24: *For the years and Stability Periods used in the text as examples, indicated by OY/SP in Column 1, the extreme value of the ΔR(MAB−ME12) distribution is given, in μm, for the analyzed ±Φ sector. The sign in front of the Φ value indicates the CMS Z side. The angle Φ is given in arc. deg. A negative sign in the ΔR value would correspond to a MAB to ME/1/2 mechanical approach while a positive value would evidence that MAB and ME/1/2 move apart. Detected motions are most probably due to instabilities of the Omron sensors.*

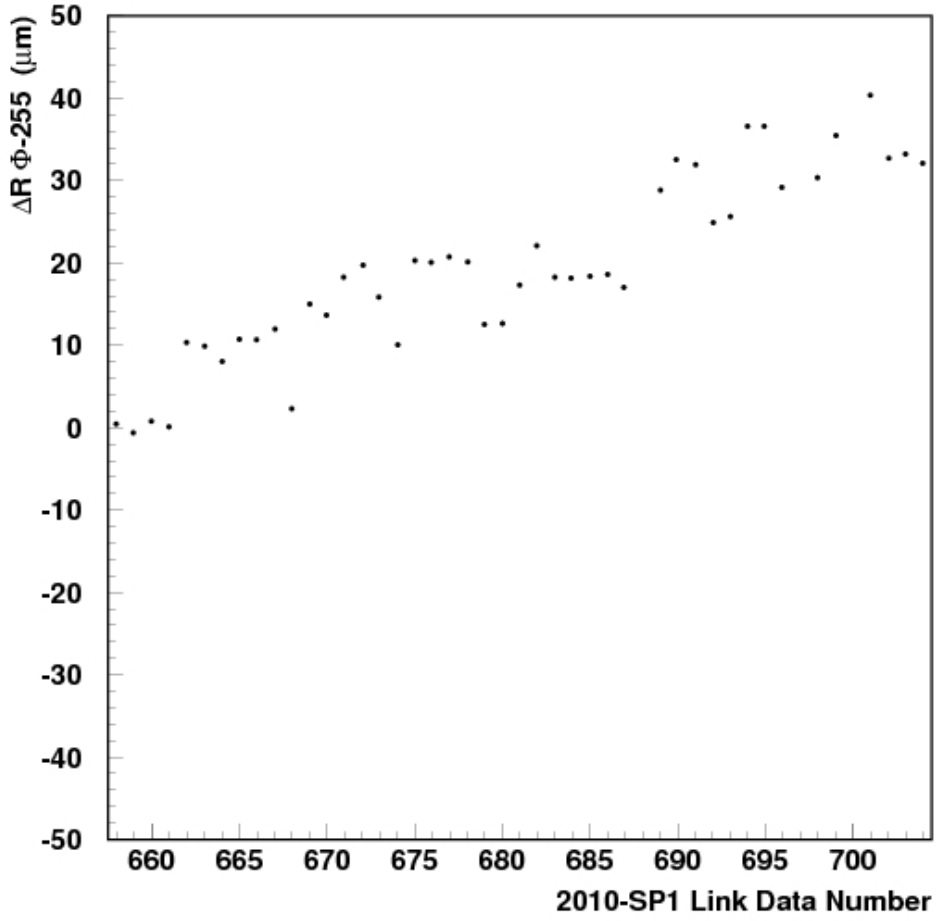

Fig. 39: *The reconstructed ΔR(MAB-ME12) (vertical axis, in μm) relative radial motion between the external MABs and their nearest ME12 endcap muon chamber as a function of the Link Data number, for the sector Φ = -255 arc. deg. during 2010−SP1.*

The data set 2013−SP1 is not as uniform as it appears in Fig. 38. The sector Φ = −15 arc. deg. is quite different from others in the same data set, as illustrated in Fig. 40.

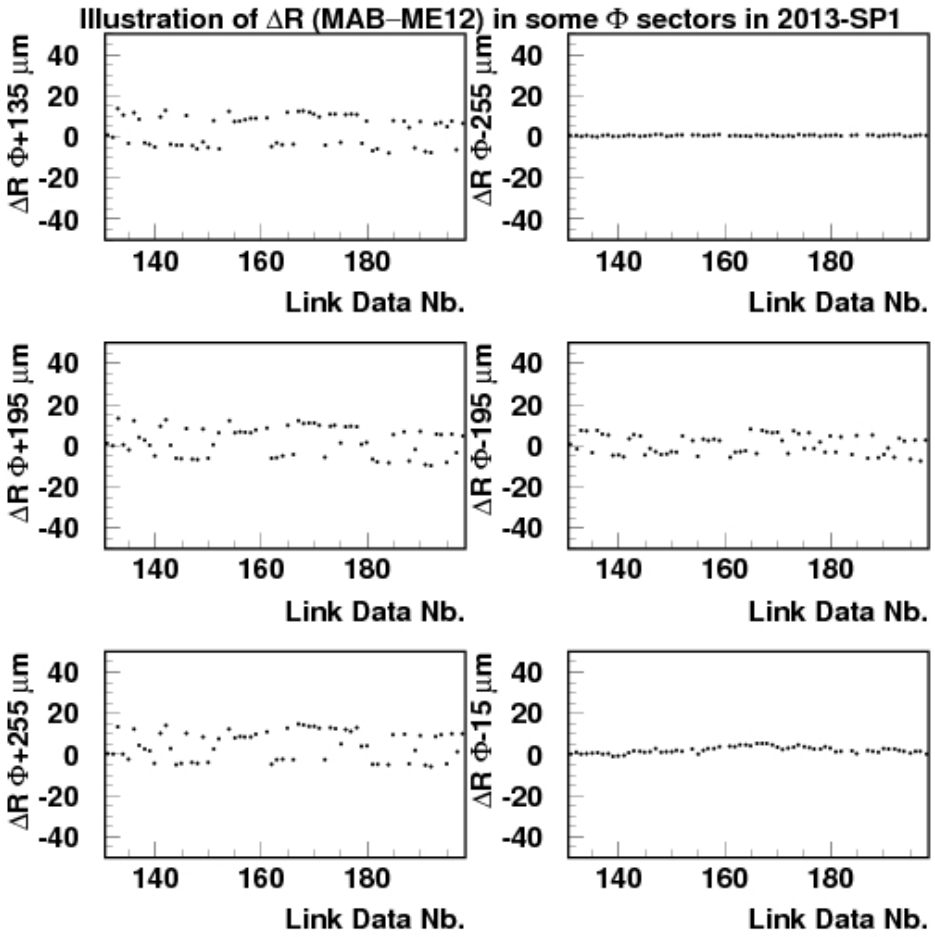

Fig. 40: *The reconstructed ΔR(MAB-ME12) (vertical axis, in μm) relative radial motion between the external MABs and their nearest ME12 endcap muon chamber as a function of the Link Data number, for some Φ = sectors during 2013–SP1.*

6.4 Measurement of Barrel Muon Chamber rotations as detected with tiltmeter sensors at the External MABs

Eventual Barrel Muon Chambers rotations in Φ are monitored with AGI [13] tiltmeter sensors, whose position at the external MABs is sketched in Fig. 5. The sensors resolution is about 30 μrad. As already said there are six external MABs at each Z end of the Barrel.

The sensor output is a voltage that is directly converted into an angle [14]. All the tiltmeters in the MABs are one dimensional sensors located in a X−Y plane, either at positive or negative values of the CMS Z coordinate. A positive increase in the output voltage translates into a ΔΦ tilt or rotation in the direction of the positive Φ. A decrease in the output voltage means a ΔΦ tilt in the direction of negative Φ. As will be shown and apart from a couple of exceptions, the detected rotations during the Stability Periods will remain below the sensor resolution, therefore compatible with mechanical stability of the Barrel Muon Chambers. However, when the current in the coil starts to increase and the field strength reaches B_{max} (4 T in 2008 and 3.8 T from 2009 on), the sensors at the external MABs (at both CMS Z sides) show clear start-up tilts that stop 24 h after Bmax is reached.

Fig. 41 illustrates those motions for some of the Magnet Cycles (MC) containing the Stability Periods investigated in this document. In Fig. 42 ΔΦ (with respect to the initial inclination of the sensor at B = 0 T) is shown as a function of the Link Data Number of the MC in question.

For the Stability periods, the ΔΦ rotations are calculated as $\Delta\Phi(MAB) = \Delta\Phi(MAB)_{data\text{-}number} - \Delta\Phi(MAB)_{initial}$ where the $\Delta\Phi(MAB)_{initial}$ value corresponds to the first data taken, at each of the twelve external MAB positions, 24 hours after B_{max} is reached in each of the OY−SP considered.

Fig. 42 illustrates, for some Φ sectors at positive and negative CMS Z sides during the considered OY−SP data taking periods, the calculated ΔΦ(MAB) relative to the AGI sensors recorded tilt as a function of the Link Data number. For this variable we have chosen the same Φ sectors as in Fig. 39, but using the one at Φ = -135° instead of Φ = -195° because of a bad operation of the corresponding tiltmeter during the 2011−SP2 data taking. Table 25 displays the extreme values of the ΔΦ(MAB) distributions for the twelve Φ sectors in the six OY−SP checked. Two records appear to be larger than the tiltmeters resolution: data set 2011−SP2, External MAB at Φ = −135 with ΔΦ = -37.3 μrad and data set 2012−SP2, External MAB at Φ = +315 with ΔΦ = -31.1 μrad, as shown on Fig. 43.

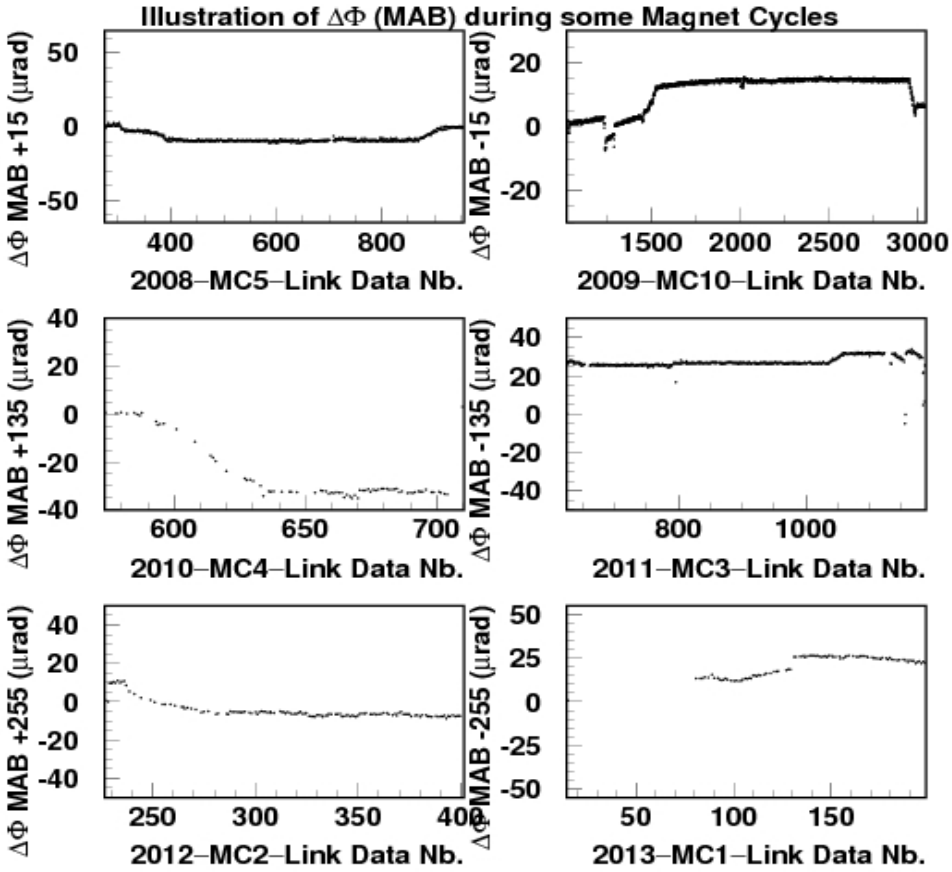

Fig 41: *Monitored ΔΦ motions (vertical axis, in μrad) for some of the Magnet Cycles (MC) containing the Stability Periods investigated in this document. ΔΦ is calculated with respect to the initial inclination of the sensor at B = 0 T and it is shown as a function of the Link Data Number of the MC in question.*

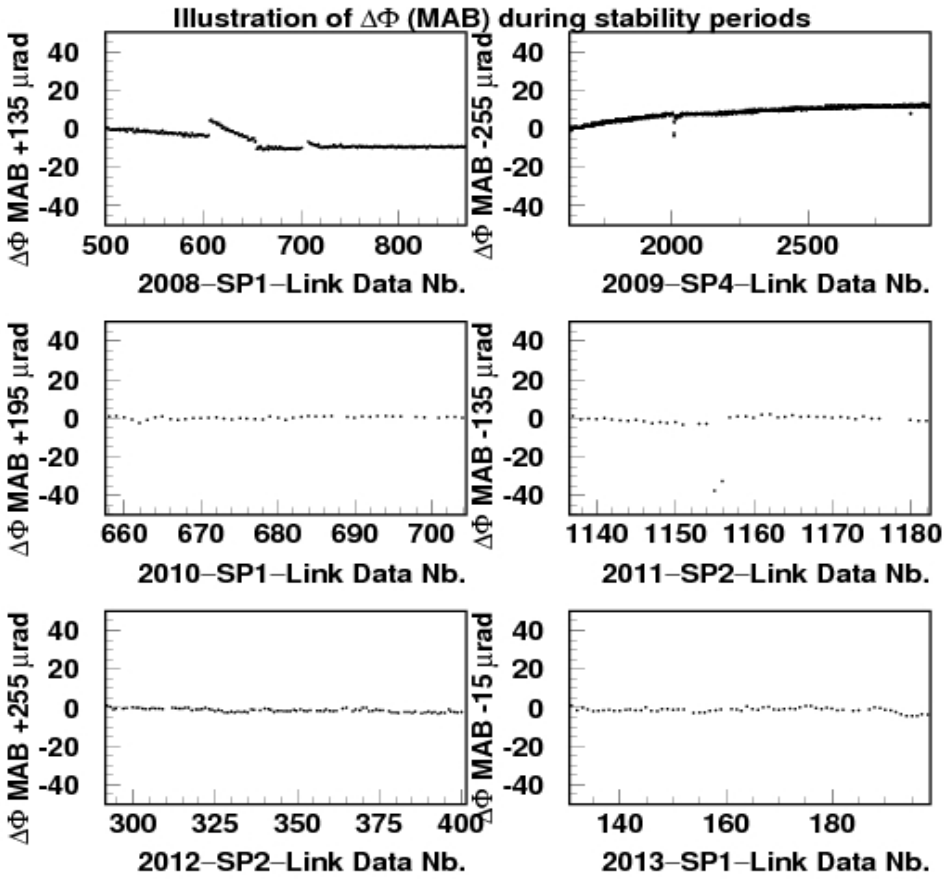

Fig. 42: *The reconstructed ΔΦ(MAB) rotations (vertical axis, in μrad) as a function of the Link Data number for some Φ sectors at positive and negative CMS Z sides during the considered OY–SP data taking periods. The sensors measuring the eventual tilts have a measured resolution of 30 μrad.*

OY/SP	±Φ/ΔR	±Φ/ΔR	±Φ/ΔR	±Φ/ΔR	±Φ/ΔR	±Φ/ΔR
2008/SP1	+15/-1.2	+75/2.7	+135/-11.2	+195/7.9	+255/-7.1	+315/12.4
	–15/15.9	–75/8.6	–135/OO	–195/OO	–255/20.0	–315/-16.7
2009/SP4	+15/-4.2	+75/2.3	+135/-15.3	+195/-3.2	+255/5.1	+315/2.7
	–15/2.8	–75/-4.7	–135/OO	–195/OO	–255/12.8	–315/-5.1
2010/SP1	+15/1.5	+75/-2.2	+135/-3.0	+195/-3.3	+255/-2.3	+315/2.3
	–15/4.5	–75/2.7	–135/OO	–195/OO	–255/-2.3	–315/-4.1
2011/SP2	+15/-5.0	+75/-3.1	+135/3.6	+195/-5.6	+255/6.5	+315/-5.8
	–15/4.7	–75/4.7	**–135/-37.3**	–195/OO	–255/-9.2	–315/OO
2012/SP2	+15/1.8	+75/-2.2	+135/-2.8	+195/2.8	+255/-5.0	**+315/-31.1**
	–15/7.9	–75/3.9	–135/-19.1	–195/-2.2	–255/2.3	–315/OO
2013/SP1	+15/3.4	+75/3.9	+135/-4.9	+195/4.9	+255/4.3	+315/5.8
	–15/-5.8	–75/-3.9	–135/-6.5	–195/-4.3	–255/-6.2	–315/OO

Table 25: *For the years and Stability Periods used in the text as examples, indicated by OY/SP in Column 1, the extreme value of the ΔΦ(MAB) distribution is given, in μrad, for the analyzed ±Φ External MAB as a function of the Link Data Number. Data are readout from AGI Tiltmeters with 30 μrad resolution.*

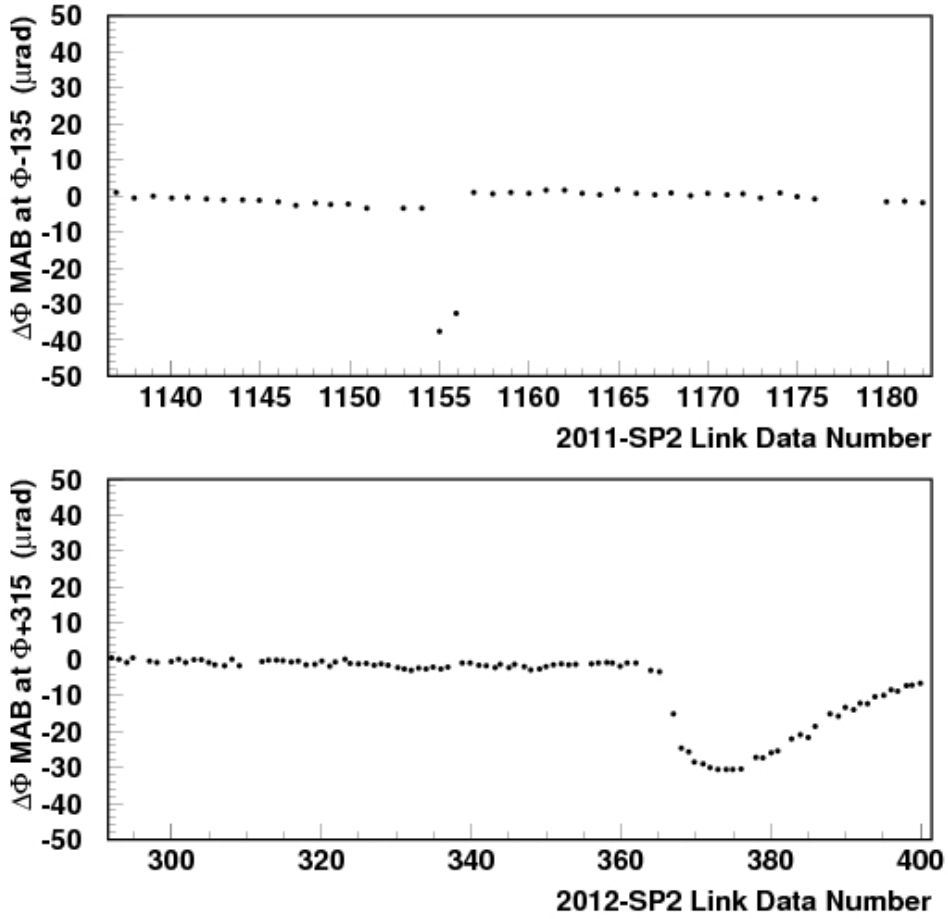

Fig. 43: *The reconstructed ΔΦ(MAB) relative angular rotations (vertical axis, in μrad) of the External MABs at Φ = -135 arc. deg. during 2011-SP2 (up) and at Φ = +315 arc. deg. during 2012-SP2 (down) as a function of their respective Link Data Numbers.*

7. Summary and conclusions

Using Link Alignment data recorded during the CRAFT08 and the CRAFT09 runs, the relative motions between various CMS mechanical structures were analyzed. The results [6-7] suggested that the CMS detector stabilizes 13.5 ± 0.5 hours after the magnetic field reaches the nominal intensity of B = 3.8 T, given that displacements between mechanical structures beyond this time do not exceed the instrumental resolution of the sensors.

A later study performed in 2010 for seven different time periods over eight months to measure motions at constant B = 3.8 T magnetic field showed that the expected mechanical stability is not observed everywhere. In particular, the relative distance $\Delta Z(\mathrm{LD}-\mathrm{AR})$ in all of the six Φ sectors exhibits variations larger than the resolution of the sensors in most of the analyzed periods [7] thus questioning the idea of an *irrevocable structural equilibrium*.

The present analysis, using the Link Alignment Data taken from the years 2008 to 2013, allows to determine that the so called out-of-stability variations detected on the $\Delta Z(\mathrm{LD}-\mathrm{AR})$ relative distance were not real, but a consequence of the systematic effects affecting the calculation of the monitored relative distances between the Link Disks and the Alignment Rings due to temperature changes during the physics data collection.

The study of 48 other variables: i) the relative axial distance between the Transfer Plates (TPs) and their nearest ME/1/1 Endcap Muon Chamber, $\Delta Z(\mathrm{TP}-\mathrm{ME11})$, ii) the relative radial distance between the external MABs and their nearest ME/1/2 Endcap Muon Chamber, $\Delta R(\mathrm{MAB}-\mathrm{ME12})$, iii) the relative radial distance between the TPs and their nearest ME/1/2, $\Delta R(\mathrm{TP}-\mathrm{ME12})$ and iv) the angular rotations of the Barrel Muon Chambers, all presumed to remain stable during the Stability Periods, showed the expected absence of displacements, nor tilts, above the sensors measurement resolutions.

Altogether, these results lead to the conclusion that CMS was mechanically stable during the full 2008 to 2013 operations at constant magnetic field, allowing an excellent muon track reconstruction.

References

[1] CMS Collaboration, “The CMS experiment at the CERN LHC”, JINST 3 (2008) S08004.
[2] The CMS Collaboration, “The Magnet Project Technical Design Report”, CERN/LHCC 97-10.
[3] The CMS Collaboration, “The Muon Project Technical Design Report”, CERN/LHCC 97-32.
[4] The CMS Collaboration, “The Tracker Project Technical Design Report”, CERN/LHCC 98-06.
[5] V. Karimaki and G. Wrochna, CMS TN/94-199; F. Matorras and A. Meneguzzo, CMS TN/95-069 and I. Belotelov et al. CMS NOTE 2006/017.
[6] L.A. García Moral et al., Nucl. Instr. and Methods A 606 (2009) 344.
[7] P. Arce et al., Nucl. Instr. And Methods A 675 (2012) 84.
[8] A. Calderón et al., Nucl. Instr. and Methods A 565 (2006) 603.
[9] A. Calderón et al., "Amorphous Silicon Position Detectors for the Link Alignment System of the CMS Detector: Users Handbook", Informe Técnico Ciemat 1126, December 2007.
[10] C. Kholer et al., Nucl. Instr. and Methods A 608 (2009) 56.
[11] Sakae Tsushin Kogyo Co., Ltd. - Trade Dept. 322 Ichinotsubo, Nakahara-ku, Kawasaki-city, Kanagawa-prefecture, 211-0016 Japan.
(htpp://www.sakae-tsushin.co.jp).
[12] Omron Corporation, Tokyo Head Office, 3-4-10 Toranomon Minato-ku, Tokyo 105, Japan. (http://www.omron.com).
[13] Applied Geomechanics Incorporated. 1336 Brommer Street, Santa Cruz, CA 95062 USA. (http://www.geomechanics.com/).
[14] J. Alberdi et al., “Tiltmeters for the Alignment System of the CMS Experiment: Users Handbook”, Informe Técnico Ciemat 1107, May 2007.
[15] P. Arce and A.L. Virto, “CMS Object Oriented Code for Optical Alignment (COCOA), CMS Note 2002/060, 2002.
[16] J.F. Fuchs, R.Goudard and J.D. Mailefaud. “CMS-Alignment, Calibration of the 3 Longitudinal Profiles (Side +)”, January 2007, CMS-MA-UR-0076.
[17] J.F. Fuchs, R.Goudard and J.D. Mailefaud. “CMS-Alignment, Calibration of the 3 Longitudinal Profiles (Side −)”, May 2007, CMS-MA-UR-0092.

1135-9420